Optimal Power Flow in Distribution Networks under $N-1$ Disruptions: A Multi-stage Stochastic Programming Approach

Haoxiang Yang, Harsha Nagarajan
Theoretical Division (T-5) and Center for Nonlinear Studies,
Los Alamos National Laboratory, NM, United States

Abstract

Contingency research to find optimal operations and post-contingency recovery plans in distribution networks has gained a major attention in recent years. To this end, we consider a multi-period optimal power flow problem in distribution networks, subject to the $N-1$ contingency where a line or distributed energy resource fails. The contingency can be modeled as a stochastic disruption, an event with random magnitude and timing. Assuming a specific recovery time, we formulate a multi-stage stochastic convex program and develop a decomposition algorithm based on stochastic dual dynamic programming. Realistic modeling features such as linearized AC power flow physics, engineering limits and battery devices with realistic efficiency curves are incorporated. We present extensive computational tests to show efficiency of our decomposition algorithm and out-of-sample performance of our solution compared to its deterministic counterpart. Operational insights on battery utilization, component hardening, and length of recovery phase are obtained by performing analyses from stochastic disruption-aware solutions.

1 Introduction

Operations accounting for a contingency recovery plan are key to ensure resilience for power networks. Most of the contingency research focuses on the transmission network since transmission contingencies require longer recovery time and potentially have a catastrophic cascading impact if no emergency adjustments are applied. To prevent such cascading impact, the $N-1$ reliability criterion[1] is widely used for transmission networks, which aims to keep normal operations for a certain time span after a single component, i.e., a line, a transformer, or a generator, fails (Bienstock 2015). On top of the $N-1$ criterion, more literature has analyzed methods and operations in the transmission network level that can mitigate contingency impact, such as capacity expansion (Choi et al. 2007), component hardening (Brown et al. 2005), post-contingency line switching (Hedman et al. 2009). As the level of distributed generation and microgrid utilization increases, contingencies in a distribution network may cause a more severe disruption at critical loads (Barnes et al. 2019, Byeon et al. 2020, Ton and Wang 2015). A distribution network has a tree structure and is operated radially, a contingency for which can potentially lead to electrical outages downstream. Furthermore, distribution systems are more vulnerable to adverse weather conditions compared to transmission systems. U.S. government sources (Executive Office of the President 2013) suggest that upgrades such as utilizing microgrids, hardening components, and incorporating $N-1$ security constraints can greatly reduce the number of outages in distribution systems during such extreme

[1] N represents the total number of network components considered for contingency analysis

events. Hence, it is important to study the resilient operations of $N-1$ compliant distribution networks.

In a distribution system, an $N-1$ contingency is a failure of a single component such as a distribution line or a distributed energy resource (DER) (Lin et al. 2019). In the previous literature (Chalil Madathil et al. 2018, Mashayekh et al. 2017, Zhou et al. 2019), the contingency may occur at every time period (15 minutes). Their primary assumption is that the disrupted component can be recovered in a single time period and a different component can fail immediately after. Such an assumption may not be reasonable since these contingencies are usually linked to infrequent, random events such as disasters (Chen 2004), and it typically takes longer than one time period to recover. Therefore, a practical model should reflect such stochastic and temporal properties of a contingency. To this end, works in Arab et al. (2015), Babaei et al. (2018) and Yuan et al. (2016) adopt realistic time-varying uncertainty sets for modeling the contingency using stochastic programming approaches. However, these approaches do not consider the component recovery time, and the recourse operations cannot be adapted for more than one contingency.

In this paper, we consider the contingency as a stochastic disruption, an event with random magnitude and timing. Recovery from the disruption lasts a certain time and in the meantime, there will not be another failure, which matches the $N-1$ setting. The magnitude of a disruption corresponds to the contingency location and the length of recovery time, and the timing of disruptions may follow some random processes (Chen 2004). Previous stochastic disruption studies focus on the single disruption case, where a two-stage stochastic program can be formulated (Salmerón et al. 2009, Yang and Morton 2019). In this paper, we allow multiple disruptions over a given time horizon, which leads to a random number of stages. Assuming the number of disruptions is small, the size of the disruption problem grows moderately in the number of time periods, which alleviates the computational burden commonly seen in a regular multi-stage stochastic program. We present a decomposition algorithm based on the well-known stochastic dynamic dual programming (SDDP) method. Our method carries a similar philosophy about the scenario tree as Algorithm 3.5 in Rebennack (2016), which proposes a scenario-based nested Benders method, but we extend the recourse problem in a general convex programming setting, prove the convergence property of our decomposition algorithm, and explore computational enhancements special to the stochastic disruption problem.

The contributions of this paper are threefold:

- to the best of our knowledge, we are the first to model multiple $N-1$ disruptions in a multi-period optimal power flow (OPF) problem accounting for recovery times in distribution networks;
- we formulate a multi-stage stochastic program, of which the length of each stage and the number of stages are both random, and we provide a computationally efficient algorithm

with convergence guarantees;

- we provide detailed numerical analyses on multiple IEEE benchmark cases with realistic modeling features and obtain operational insights.

This paper is an extended version of the conference proceedings paper (Yang and Nagarajan 2020) in two substantial ways: (i) it provides a detailed proof of the convexity, the relatively complete recourse, and the asymptotic convergence of the decomposition method; and (ii) it includes larger test cases, shows potential enhancement in the cut generation process and presents more comprehensive computational results, such as the gap between the lower bound and the objective value of simulated scenarios.

In Section 2, we describe the modeling features and formulate the multi-stage stochastic program for the OPF in distribution networks under stochastic $N-1$ disruptions. We then propose an SDDP-based decomposition algorithm and prove its asymptotic convergence in Section 3. Detailed numerical results are presented in Section 4 including computational improvements, cost comparison against alternative policies and what-if analyses.

2 Problem Formulation

Nomenclature

Indices and index sets

$\mathcal{N}$	set of buses, indexed by i
$\mathcal{E}$	set of lines, indexed by ij as the line between bus i and j
$\mathcal{G}$	set of generators, indexed by g
$\mathcal{G}_i \subseteq \mathcal{G}$	subset of generators at bus i
$i_g \in \mathcal{N}$	bus where generator $g \in \mathcal{G}$ is located
$\mathcal{B}$	set of batteries, indexed by b
$\mathcal{B}_i \subseteq \mathcal{B}$	subset of batteries at bus i
$i_b \in \mathcal{N}$	bus where battery $b \in \mathcal{B}$ is located
$\mathcal{T}$	set of time periods $= \{1, \dots, T\}$, indexed by t
Ω	set of disruption scenarios, indexed by ω
$\mathcal{L}_b$	set of pieces of battery efficiency curve at battery b, indexed by ℓ_b

Parameters

d^p_{it}, d^q_{it}	active and reactive power demand at bus $i \in \mathcal{N}$ at time $t \in \mathcal{T}$, (MW, MVAr)
R_{ij}, X_{ij}	resistance and reactance of line $ij \in \mathcal{E}$, $(k\Omega)$
$\underline{V}_i, \bar{V}_i$	squared voltage lower and upper bound at bus $i \in \mathcal{N}$, $((kV)^2)$
c^B_b	battery apparent power generation capacity cost, (\$/(MVA))
c^l	load mismatch penalty, (\$/(MW), \$/(MVAr))

$c_{g,1}, c_{g,2}$	linear and quadratic operational cost for generator $g \in \mathcal{G}$, respectively, ($/MW, $/(MW)^2)
W_{ij}	apparent power thermal limit on line $ij \in \mathcal{E}$, (MVA)
$\bar{s}^p_g, \bar{s}^q_g$	maximum active and reactive power generated by generator $g \in \mathcal{G}$, (MW, MVAr)
$\underline{s}^p_g, \underline{s}^q_g$	minimum active and reactive power generated by generator $g \in \mathcal{G}$, (MW, MVAr)
R^U_g, R^D_g	up and down ramp rates for generator $g \in \mathcal{G}$, (MW/h)
$\bar{I}_b$	max. energy storage capacity of the battery b, (MWh)
$\alpha^\ell_b, \beta^\ell_b$	slope and y-axis intercept of the piece $\ell \in \mathcal{L}_b$ in the battery efficiency curve for battery $b \in \mathcal{B}$
$\bar{u}_b$	upper bound on the apparent power output capacity for battery $b \in \mathcal{B}$, (MVA)
Δt	time step, (h)
τ^ω	recovery time in the number of time steps for scenario ω
t_D	time of disruption
B^ω_{gt}	1 if generator g fails at time t with disruption scenario ω, 0 otherwise
B^ω_{ijt}	1 if line ij fails at time t with disruption scenario ω, 0 otherwise
p^ω_t	probability of the disruption scenario $\omega \in \Omega$ occurring in $t = 1, 2, \ldots, T$ time period after the earliest possible disruption time

Decision variables

s^p_{gt}, s^q_{gt}	active and reactive power generation during time $t \in \mathcal{T}$ from generator $g \in \mathcal{G}$, (MW, MVAr)
V_{it}	squared voltage at bus $i \in \mathcal{N}$ at time $t \in \mathcal{T}$, ($(kV)^2$)
P_{ijt}, Q_{ijt}	active and reactive power flow though line $ij \in \mathcal{E}$ at time $t \in \mathcal{T}$, (MW, MVAr)
u_b	apparent power output capacity for battery $b \in \mathcal{B}$, (MVA)
w_{bt}	state-of-charge in battery $b \in \mathcal{B}$ at time $t \in \mathcal{T}$, (MWh)
z^p_{bt}, z^q_{bt}	actual active and reactive power output during time $t \in \mathcal{T}$ from battery $b \in \mathcal{B}$, (MW, MVAr)
y_{bt}	active power output before losses during time $t \in \mathcal{T}$ from battery $b \in \mathcal{B}$, (MW)
L^{p+}_{it}, L^{q+}_{it}	active and reactive power load shedding during time $t \in \mathcal{T}$ at bus $i \in \mathcal{N}$, (MW, MVAr)
L^{p-}_{it}, L^{q-}_{it}	active and reactive power load compensation during time $t \in \mathcal{T}$ at bus $i \in \mathcal{N}$, (MW, MVAr)

First we introduce the notation for the multi-period OPF problem in a distribution network under stochastic $N-1$ disruptions. The distribution network is represented by a graph $(\mathcal{N}, \mathcal{E})$, where $\mathcal{N}$ is the set of buses and $\mathcal{E}$ is the set of lines. This network is the standard representation used for modeling power flow physics (Cain et al. 2012). At bus $i \in \mathcal{N}$ there is a set of generators, $\mathcal{G}_i$, and a set of batteries, $\mathcal{B}_i$. For each generator, we assume an active power ramping limit between two adjacent time periods, which is consistent with the literature (Frangioni and Gentile 2006). In addition, we assume $\underline{s}^p_g = 0, \forall g \in \mathcal{G}$, which guarantees that the active generation will be feasible under the ramping constraints after a generator recovers from a failure. Each battery $b \in \mathcal{B}$ has a given energy capacity but the maximum apparent power output is a decision variable (u_b). Power

loss associated to charging and discharging can be modeled by a piecewise linear efficiency curve between the pre-loss active power output, y_{bt}, and the actual active power output, z^p_{bt}; see Bienstock et al. (2016), Chalil Madathil et al. (2018), Hari et al. (2018) for detailed descriptions of battery features. Since the battery efficiency curve itself is piecewise linear, which is typically modeled using additional binary variables, we instead use area underneath the curve as a polyhedral relaxation of the piecewise curve. The illustration of the battery efficiency curve and the polyhedral relaxation is shown in Figure 1. We assume that the battery efficiency curve passes through the origin as the standby loss is negligible.

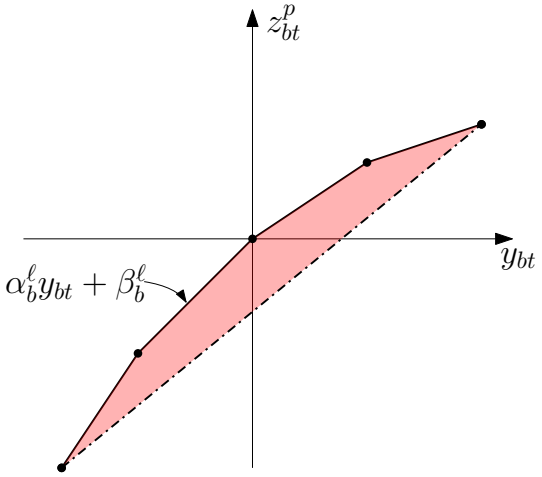

Figure 1: Battery efficiency curve of battery $b \in \mathcal{B}$ at time period t is represented using solid line and the polyhedral (convex) relaxation corresponds to the red shaded region underneath the curve.

The demand at each bus is assumed deterministic throughout the time horizon $\mathcal{T}$, but a line or a generator can fail at a random time, which from now on shall be referred to as a *disruption*. Given an observed scenario ω, recovery takes certain time periods, τ^ω, during which the system will not suffer from another disruption. For example, if a disruption occurs at time period 3 and $\tau^\omega = 2$, the subsequent disruption can only occur after time period 5. Given the earliest possible disruption time t', the probability distribution is characterized by a mass function with a finite support, p^ω_t, i.e., the probability of observing disruption scenario ω at time period $t' + t$ is p^ω_t. In other words, the random variable of the time span between t' and the next realized disruption is conditionally independent of the history given t'. Since we are only concerned with a disruption occurring within the time horizon, we can assume that t is upper bounded by T.

We aim to minimize the expected total cost, which includes the battery capacity cost, the generation cost and the energy mismatch penalty cost. The battery capacity cost is linear in the maximum apparent power output, $u_b, \forall b \in \mathcal{B}$, and is incurred in the beginning. The generation cost is a quadratic function of active power generation. Due to disruptions and ramping constraints, a load mismatch may have to be incurred to keep the system feasible. Suppose a symbol without a sub-

script represents a vector. The load mismatch is denoted by non-negative variables, L^{p+}, L^{p-}, L^{q+} and L^{q-}, and penalized by a penalty cost c^l. In summary, we let $C_{t_1,t_2}(s^p, L^{p+}, L^{p-}, L^{q+}, L^{q-})$ be the sum of generation costs and load mismatch costs between time t_1 and time t_2:

$$C_{t_1,t_2}(s^p, L^{p+}, L^{p-}, L^{q+}, L^{q-}) = \sum_{t=t_1}^{\min\{t_2,T\}} \left[\sum_{i\in\mathcal{N}} c^l \left(L^{p+}_{it} + L^{p-}_{it} + L^{q+}_{it} + L^{q-}_{it} \right) + \sum_{g\in\mathcal{G}} \left(c_{g,2}(s^p_{gt})^2 + c_{g,1} s^p_{gt} \right) \right].$$

Given a disruption scenario ω occurring at time period t, we denote the future cost function as $f^\omega_t(s^p_{\cdot t-1}, w_{\cdot t-1}, u)$, where $\cdot$ in the subscript represents a vector including all indices in the corresponding set; e.g., $s^p_{\cdot t-1} = \{s^p_{gt-1} \mid g \in \mathcal{G}\}$. Suppose a disruption of scenario ω is observed at time t. This definition means that the optimal expected operational cost between time t and the end of the time horizon is a function of the state of the system entering time t, $(s^p_{\cdot t-1}, w_{\cdot t-1}, u)$. The value function can be considered as an equivalent to the cost-to-go function in a dynamic programming narrative. Throughout the paper we make further assumptions:

A.1 There are two independent probability distributions: p_t represents the probability of the time span between the earliest possible disruption time and the next disruption time equals to t, $t = 1, 2, \ldots, T$, and p^ω represents the probability of observing scenario ω, $\omega \in \Omega$. This is equivalent to $p^\omega_t = p_t p^\omega, \forall t = 1, 2, \ldots, T, \omega \in \Omega$.

A.2 The future function cost, f^ω_t, is conditionally independent of previous disruptions and decisions, $(s^p_{\cdot t'}, s^q_{\cdot t'}, V_{\cdot t'}, P_{\cdot t'}, Q_{\cdot t'}, z^p_{\cdot t'}, z^q_{\cdot t'}, y_{\cdot t'}, w_{\cdot t'}, L^{p+}_{\cdot t'}, L^{p-}_{\cdot t'}, L^{q+}_{\cdot t'}, L^{q-}_{\cdot t'}), \forall t' = 1, \ldots, t-2$, given $(s^p_{\cdot t-1}, w_{\cdot t-1}, u)$.

A.3 Function $f^\omega_t(s^p_{\cdot t-1}, w_{\cdot t-1}, u) = 0, \forall \omega \in \Omega, t > T$, if $s^p_{gt-1} \in [\underline{s}^p_g, \bar{s}^p_g], \forall g \in \mathcal{G}$, $w_{bt-1} \in [0, \bar{I}_b], \forall b \in \mathcal{B}$ and $u \in [0, \bar{u}_b], \forall b \in \mathcal{B}$.

A.4 $c_{g,2} \geq 0, \forall g \in \mathcal{G}$.

Assumption A.1 is an approximation that each component's failure follows an independent arrival process, e.g., a Poisson process, and we superposition them across $\omega \in \Omega$ to obtain the probability measure p_t, with each component's failure rate proportional to p^ω; see Chen (2004) for detailed probability models of power system failures. Assumption A.2 matches the $N-1$ contingency setting, since the system is recovered when it is possible to observe a disruption at time t, and only the state variables, (s^p, w, u), are required information for future operations. Assumption A.3 states that we limit our concern to the operations within the time horizon, beyond which the cost is zero. Assumption A.4 implies that all C functions are convex since the coefficients for the quadratic terms are non-negative, thus keeping it consistent with the power systems literature (Bandi et al. 2019).

The optimization model can be presented in a nested formulation as follows:

$$z^* = \min \quad \sum_{b\in\mathcal{B}} c_b^B u_b + \sum_{t=1}^{T}\sum_{\omega\in\Omega} p_t^\omega \left[C_{1,t}(s^p, L^{p+}, L^{p-}, L^{q+}, L^{q-}) + f_{1+t}^\omega(s_{\cdot t}^p, w_{\cdot t}, u)\right] \tag{1a}$$

$$\text{s.t.} \quad \sum_{b\in\mathcal{B}_i} z_{bt}^p + \sum_{g\in\mathcal{G}_i} s_{gt}^p - d_{it}^p + L_{it}^{p+} - L_{it}^{p-} = \sum_{ij\in\mathcal{E}} P_{ijt} \qquad \forall\, i\in\mathcal{N}, t\in\mathcal{T} \tag{1b}$$

$$\sum_{b\in\mathcal{B}_i} z_{bt}^q + \sum_{g\in\mathcal{G}_i} s_{gt}^q - d_{it}^q + L_{it}^{q+} - L_{it}^{q-} = \sum_{ij\in\mathcal{E}} Q_{ijt} \qquad \forall\, i\in\mathcal{N}, t\in\mathcal{T} \tag{1c}$$

$$(P_{ijt})^2 + (Q_{ijt})^2 \le W_{ij}^2 \qquad \forall\, ij\in\mathcal{E}, t\in\mathcal{T} \tag{1d}$$

$$V_{jt} = V_{it} - 2\left(R_{ij}P_{ijt} + X_{ij}Q_{ijt}\right) \qquad \forall\, ij\in\mathcal{E}, t\in\mathcal{T} \tag{1e}$$

$$R_g^D \le s_{gt}^p - s_{gt-1}^p \le R_g^U \qquad \forall\, g\in\mathcal{G}, t=2,\ldots,T \tag{1f}$$

$$\underline{s}_g^p \le s_{gt}^p \le \bar{s}_g^p \qquad \forall\, g\in\mathcal{G}, t\in\mathcal{T} \tag{1g}$$

$$\underline{s}_g^q \le s_{gt}^q \le \bar{s}_g^q \qquad \forall\, g\in\mathcal{G}, t\in\mathcal{T} \tag{1h}$$

$$\underline{V}_i \le V_{it} \le \bar{V}_i \qquad \forall\, i\in\mathcal{N}, t\in\mathcal{T} \tag{1i}$$

$$w_{bt} = w_{bt-1} - y_{bt}\Delta_t \qquad \forall\, b\in\mathcal{B}, t\in\mathcal{T} \tag{1j}$$

$$\left(z_{bt}^p\right)^2 + \left(z_{bt}^q\right)^2 \le u_b^2 \qquad \forall\, b\in\mathcal{B}, t\in\mathcal{T} \tag{1k}$$

$$z_{bt}^p \le \alpha_b^\ell y_{bt} + \beta_b^\ell \qquad \forall\, b\in\mathcal{B}, \ell\in\mathcal{L}_b, t\in\mathcal{T} \tag{1l}$$

$$0 \le w_{bt} \le \bar{I}_b \qquad \forall\, b\in\mathcal{B}, t\in\mathcal{T} \tag{1m}$$

$$0 \le u_b \le \bar{u}_b \qquad \forall\, b\in\mathcal{B} \tag{1n}$$

$$L_{it}^{p+}, L_{it}^{p-}, L_{it}^{q+}, L_{it}^{q-} \ge 0 \qquad \forall\, i\in\mathcal{N}, t\in\mathcal{T}. \tag{1o}$$

At each time period, the operations decisions include active and reactive generations, battery charges, discharges and storage, line power flows, bus voltages and load mismatches. We can consider the solution to model (1) as a nominal plan: although we model the decisions from time period 1 to T, we implement such solution only until the first disruption is realized. In model (1), constraints (1b) and (1c) model active and reactive power balance at all buses, and constraint (1d) ensures that apparent power flows do not exceed thermal limits. Constraint (1e) characterizes the power flow equation under the *LinDistFlow* setting, which is a simple yet reasonable approximation under some mild assumptions, e.g., balanced loads for distribution networks (Baran and Wu 1989, Gan et al. 2014); see Vanin et al. (2020) for *LinDistFlow*'s performance in comparison to the second-order conic based relaxations and original non-linear non-convex formulation on multi-phase radial networks. Constraint (1f) models generators' ramping up/down limits. Constraints (1g),(1h) and (1i) enforce the bounds on active generation, reactive generation and bus voltages, respectively. Constraint (1j) models time coupling for battery state-of-charge and constraint (1k) models the apparent power output limit from a battery. Constraint (1l) characterizes the relaxation of battery efficiency curves as shown in Figure 1. Constraints (1m) and (1n) bound the storage and apparent

power output capacity of a battery. The maximum energy storage capacity, $\bar{I}_b$, is estimated based on the implied bounds from the worst-case values attained by the upper bound of the apparent power output capacity (u_b) variable (Chalil Madathil et al. 2018, Hari et al. 2018). Non-negative load mismatch variables are indicated in constraint (1o).

The objective function (1a) minimizes the expected total cost. The battery capacity cost is incurred before the first time period. For a specific disruption scenario ω occurring at time period $1+t$, the cost includes generation and load mismatch costs between time 1 and t, and the future costs conditioned on the disruption. Given a disruption time, t_D, and a disruption scenario, ω, the future cost function can be formulated in model (2):

$$f^{\omega}_{t_D}(\hat{s}^p_{\cdot t_D-1}, \hat{w}_{\cdot t_D-1}, \hat{u}) = \min \sum_{t=1}^{T} \sum_{\omega\in\Omega} p^{\omega}_t \left[C_{t_D, t_D+\tau^\omega+t-1}(s^p, L^{p+}, L^{p-}, L^{q+}, L^{q-}) + f^{\omega}_{t_D+\tau^\omega+t}(s^p_{\cdot t_D+\tau^\omega+t-1}, w_{\cdot t_D+\tau^\omega+t-1}, u)\right] \tag{2a}$$

$$\text{s.t.} \quad \sum_{b\in\mathcal{B}_i} z^p_{bt} + \sum_{g\in\mathcal{G}_i} s^p_{gt} - d^p_{it} + L^{p+}_{it} - L^{p-}_{it} = \sum_{ij\in\mathcal{E}} P_{ijt} \qquad \forall\, i\in\mathcal{N}, t = t_D,\dots,T \tag{2b}$$

$$\sum_{b\in\mathcal{B}_i} z^q_{bt} + \sum_{g\in\mathcal{G}_i} s^q_{gt} - d^q_{it} + L^{q+}_{it} - L^{q-}_{it} = \sum_{ij\in\mathcal{E}} Q_{ijt} \qquad \forall\, i\in\mathcal{N}, t = t_D,\dots,T \tag{2c}$$

$$(P_{ijt})^2 + (Q_{ijt})^2 \le (1 - B^{\omega}_{ijt}) W^2_{ij} \qquad \forall\, ij\in\mathcal{E}, t = t_D,\dots,T \tag{2d}$$

$$V_{jt} - V_{it} \le -2\left(R_{ij}P_{ijt} + X_{ij}Q_{ijt}\right) + B^{\omega}_{ijt}M \qquad \forall\, ij\in\mathcal{E}, t = t_D,\dots,T \tag{2e}$$

$$V_{jt} - V_{it} \ge -2\left(R_{ij}P_{ijt} + X_{ij}Q_{ijt}\right) - B^{\omega}_{ijt}M \qquad \forall\, ij\in\mathcal{E}, t = t_D,\dots,T \tag{2f}$$

$$s^p_{gt} - s^p_{gt-1} \ge R^D_g - B^{\omega}_{gt}M \qquad \forall\, g\in\mathcal{G}, t = t_D,\dots,T \tag{2g}$$

$$s^p_{gt} - s^p_{gt-1} \le R^U_g + B^{\omega}_{gt}M \qquad \forall\, g\in\mathcal{G}, t = t_D,\dots,T \tag{2h}$$

$$\underline{s}^p_g(1 - B^{\omega}_{gt}) \le s^p_{gt} \le \bar{s}^p_g(1 - B^{\omega}_{gt}) \qquad \forall\, g\in\mathcal{G}, t = t_D,\dots,T \tag{2i}$$

$$\underline{s}^q_g(1 - B^{\omega}_{gt}) \le s^q_{gt} \le \bar{s}^q_g(1 - B^{\omega}_{gt}) \qquad \forall\, g\in\mathcal{G}, t = t_D,\dots,T \tag{2j}$$

$$\underline{V}_i \le V_{it} \le \bar{V}_i \qquad \forall\, i\in\mathcal{N}, t = t_D,\dots,T \tag{2k}$$

$$w_{bt} = w_{bt-1} - y_{bt}\Delta_t \qquad \forall\, b\in\mathcal{B}, t = t_D,\dots,T \tag{2l}$$

$$\left(z^p_{bt}\right)^2 + \left(z^q_{bt}\right)^2 \le u^2_b \qquad \forall\, b\in\mathcal{B}, t = t_D,\dots,T \tag{2m}$$

$$z^p_{bt} \le \alpha^{\ell}_b y_{bt} + \beta^{\ell}_b \qquad \forall\, b\in\mathcal{B}, \ell\in\mathcal{L}_b, t = t_D,\dots,T \tag{2n}$$

$$0 \le w_{bt} \le \bar{I}_b \qquad \forall\, b\in\mathcal{B}, t = t_D,\dots,T \tag{2o}$$

$$0 \le u_b \le \bar{u}_b \qquad \forall\, b\in\mathcal{B} \tag{2p}$$

$$L^{p+}_{it}, L^{p-}_{it}, L^{q+}_{it}, L^{q-}_{it} \ge 0 \qquad \forall\, i\in\mathcal{N}, t = t_D,\dots,T \tag{2q}$$

$$s^p_{gt_D-1} = \hat{s}^p_{gt_D-1} \qquad \forall\, g\in\mathcal{G} \tag{2r}$$

$$w_{bt_D-1} = \hat{w}_{bt_D-1} \qquad \forall\, b\in\mathcal{B} \tag{2s}$$

$$u_b = \hat{u}_b \qquad \forall\, b\in\mathcal{B}. \tag{2t}$$

We distinguish the first-stage model (1) and later-stage model (2) because (i) the battery ca-

pacity decisions have to be made in the beginning; and (ii) the later stages observe disruption and have to follow the non-anticipativity rule. The solution to model (2) will be carried out until the next disruption, given that a disruption of scenario ω has just occurred at time period t_D. Constraints (2b)-(2q) replicate constraints (1b)-(1o) with the indices adjusted to the correct time horizon starting from the disruption. The value of indicator parameters B^{ω}_{ijt} and B^{ω}_{gt} characterizes the realized disruption scenario, as shown in constraints (2d)-(2j). For example, if the disruption occurs at line ij under the scenario ω at time t_D, then for the recovery time periods $t' = t_D, \ldots, t_D + \tau^{\omega}$, $B^{\omega}_{ijt'} = 1$, and all other $B_{ijt'}$ and $B_{gt'}$ parameters take value 0. With M being a large number, when $B^{\omega}_{ijt} = 1$ for some line ij, the apparent power thermal limit is set to 0 and the power flow equation is deactivated. Similarly, when $B^{\omega}_{gt} = 1$ for some generator g, the amount of real/reactive generation is enforced at 0 and the ramping constraints are relaxed. Constraints (2r)-(2t) are non-anticipativity constraints which ensure that the solutions after observing the current disruption must be consistent with the solutions that have been implemented already. The linking variables, which are called the "state variables", include active power generations and batteries' state-of-charge and apparent power output capacity.

We can prove our models have relatively complete recourse and convexity, which are useful properties to ensure tractability (Shapiro et al. 2009). First, the problem is meaningful only if the following feasibility assumption is true, that there is a feasible operation point when the distribution network is not disrupted.

A.5 Model (1) has a feasible region with a nonempty relative interior.

With Assumption A.5, model (2) is always feasible, regardless of the value of the state variables, which from the addition of load mismatch variables, L^{p+}, L^{p-}, L^{q+} and L^{q-}. We show this feasibility result in Lemma 1 by constructing a feasible solution to model (2).

Lemma 1. *For any pair of (t, ω) where $t = 2, 3, \ldots$ and $\omega \in \Omega$, suppose $\hat{s}^{p}_{\cdot t-1}$, $\hat{w}_{\cdot t-1}$ and $\hat{u}$ satisfies the constraints:*

$$\hat{s}^{p}_{gt-1} \in [\underline{s}^{p}_{g}, \bar{s}^{p}_{g}] \;\; g \in \mathcal{G}, \qquad \hat{w}_{bt-1} \in [0, \bar{I}_b] \;\; b \in \mathcal{B}, \qquad \hat{u}_b \in [0, \bar{u}_b] \;\; b \in \mathcal{B}. \tag{3}$$

Then, $f^{\omega}_{t}(\hat{s}^{p}_{\cdot t-1}, \hat{w}_{\cdot t-1}, \hat{u}) < +\infty$.

Proof. We use backward induction to prove this lemma. Suppose it is true that given a t, for all $t' \geq t, \omega \in \Omega$, we have $f^{\omega}_{t'}(\hat{s}^{p}_{\cdot t'-1}, \hat{w}_{\cdot t'-1}, \hat{u}) < +\infty$ for $(\hat{s}^{p}_{\cdot t'-1}, \hat{w}_{\cdot t'-1}, \hat{u})$ satisfying conditions (3). As Assumption A.5 suggests, we can find a feasible solution for model (1), of which the voltages and power flows denoted as $\tilde{V}, \tilde{P}$ and $\tilde{Q}$. Then this hypothesis is true for $t = T$, because for all $t' > T$, all future value functions equal to zero according to Assumption A.3, and for $t' = T$, given $(\hat{s}^{p}_{\cdot T-1}, \hat{w}_{\cdot T-1}, \hat{u})$ satisfying constraints (3), we can construct a feasible solution for all $\omega \in \Omega$ as:

$$s^{p}_{gT} = \begin{cases} 0 & \text{if } B^{\omega}_{gT} = 1 \\ \hat{s}^{p}_{gT-1} & \text{otherwise} \end{cases} \qquad s^{q}_{gT} = \begin{cases} 0 & \text{if } B^{\omega}_{gT} = 1 \\ \underline{s}^{q}_{g} & \text{otherwise} \end{cases} \qquad \forall g \in \mathcal{G} \tag{4a}$$

$$V_{iT} = \tilde{V}_{iT} \qquad \forall i \in \mathcal{N} \tag{4b}$$

$$P_{ijT} = \begin{cases} 0 & \text{if } B^{\omega}_{ijT} = 1 \\ \tilde{P}_{ijT} & \text{otherwise} \end{cases} \qquad Q_{ijT} = \begin{cases} 0 & \text{if } B^{\omega}_{ijT} = 1 \\ \tilde{Q}_{ijT} & \text{otherwise} \end{cases} \qquad \forall ij \in \mathcal{E} \tag{4c}$$

$$w_{bT} = \hat{w}_{bT-1} \qquad z^p_{bT} = z^q_{bT} = y_{bT} = 0 \qquad u_b = \hat{u}_b \qquad \forall b \in \mathcal{B} \tag{4d}$$

$$\phi^p_{iT} = d^p_{iT} - \sum_{g \in \mathcal{G}_i} s^p_{gT} + \sum_{ij \in \mathcal{E}} P_{ijT} \qquad \phi^q_{iT} = d^q_{iT} - \sum_{g \in \mathcal{G}_i} s^q_{gT} + \sum_{ij \in \mathcal{E}} Q_{ijT} \qquad \forall i \in \mathcal{N} \tag{4e}$$

$$L^{p+}_{iT} = \max\{\phi^p_{iT}, 0\} \qquad L^{p-}_{iT} = \max\{-\phi^p_{iT}, 0\} \qquad \forall i \in \mathcal{N} \tag{4f}$$

$$L^{q+}_{iT} = \max\{\phi^q_{iT}, 0\} \qquad L^{q-}_{iT} = \max\{-\phi^q_{iT}, 0\} \qquad \forall i \in \mathcal{N}. \tag{4g}$$

Notice that constraints (2g) and (2h) hold because $0 \in [\underline{s}^p_g, \bar{s}^p_g], \forall g \in \mathcal{G}$, and constraints (2n) hold because the battery efficiency curve passes the origin, i.e., there exists an $\ell \in \mathcal{L}_b$ for every $b \in \mathcal{B}$ such that $\beta^\ell_b = 0$.

Now, we prove that for $t-1$, if the hypothesis is true for time t and $(\hat{s}^p_{\cdot t-2}, \hat{w}_{\cdot t-2}, \hat{u})$ satisfies condition (3), we have $f^{\omega}_{t-1}(\hat{s}^p_{\cdot t-2}, \hat{w}_{\cdot t-2}, \hat{u}) < +\infty$. Similarly, we can construct a feasible solution for all $\omega \in \Omega$ as:

$$s^p_{gt'} = \begin{cases} 0 & \text{if } B^{\omega}_{gt-1} = 1 \\ \hat{s}^p_{gt-2} & \text{otherwise} \end{cases} \qquad s^q_{gt'} = \begin{cases} 0 & \text{if } B^{\omega}_{gt-1} = 1 \\ \underline{s}^q_g & \text{otherwise} \end{cases} \qquad \forall t' = t-1, \ldots, T, g \in \mathcal{G} \tag{5a}$$

$$V_{it'} = \tilde{V}_{it'} \qquad \forall t' = t-1, \ldots, T, i \in \mathcal{N} \tag{5b}$$

$$P_{ijt'} = \begin{cases} 0 & \text{if } B^{\omega}_{ijt'} = 1 \\ \tilde{P}_{ijt'} & \text{otherwise} \end{cases} \qquad Q_{ijt'} = \begin{cases} 0 & \text{if } B^{\omega}_{ijt'} = 1 \\ \tilde{Q}_{ijt'} & \text{otherwise} \end{cases} \qquad \forall t' = t-1, \ldots, T, ij \in \mathcal{E} \tag{5c}$$

$$w_{bt'} = \hat{w}_{bt-2} \qquad z^p_{bt'} = z^q_{bt'} = y_{bt'} = 0 \qquad \forall t' = t-1, \ldots, T, b \in \mathcal{B} \tag{5d}$$

$$u_b = \hat{u}_b \qquad \forall b \in \mathcal{B} \tag{5e}$$

$$\phi^p_{ijt'} = d^p_{it'} - \sum_{g \in \mathcal{G}_i} s^p_{gt'} + \sum_{ij \in \mathcal{E}} P_{ijt'} \qquad \forall t' = t-1, \ldots, T, i \in \mathcal{N} \tag{5f}$$

$$\phi^q_{ijt'} = d^q_{it'} - \sum_{g \in \mathcal{G}_i} s^q_{gt'} + \sum_{ij \in \mathcal{E}} Q_{ijt'} \qquad \forall t' = t-1, \ldots, T, i \in \mathcal{N} \tag{5g}$$

$$L^{p+}_{it'} = \max\{\phi^p_{ijt'}, 0\} \qquad L^{p-}_{it'} = \max\{-\phi^p_{ijt'}, 0\} \qquad \forall t' = t-1, \ldots, T, i \in \mathcal{N} \tag{5h}$$

$$L^{q+}_{it'} = \max\{\phi^q_{ijt'}, 0\} \qquad L^{q-}_{it'} = \max\{-\phi^q_{ijt'}, 0\} \qquad \forall t' = t-1, \ldots, T, i \in \mathcal{N}. \tag{5i}$$

Since $(\hat{s}^p_{gt-2}, \hat{w}_{\cdot t-2}, \hat{u})$ satisfies condition (3), according to this construction, $(s^p_{gt'}, w_{\cdot t'}, u)$ also satisfies condition (3) for every $t' = t-1, \ldots, T$. As the hypothesis is true for t, all $f^{\omega}_{t'}(s^p_{gt'}, w_{\cdot t'}, u) < +\infty$ for all $t' = t-1, \ldots, T$; therefore, for the constructed solution, we yield a finite objective function value, which indicates that the hypothesis is true for $t-1$. By induction, we can complete the proof that for every $t \geq 2$, $f^{\omega}_t(\hat{s}^p_{\cdot t-1}, \hat{w}_{\cdot t-1}, \hat{u}) < +\infty$ for all $\omega \in \Omega$ given a solution $(\hat{s}^p_{\cdot t-1}, \hat{w}_{\cdot t-1}, \hat{u})$ satisfying condition (3). □

We can define the explicit constraint sets and the induced feasible sets for each stage of the problem as follows:

Definition 1. *For simplicity, we use the notation x_t to represent the collection of decisions, $(s^p_{\cdot t}, s^q_{\cdot t}, V_{\cdot t}, P_{\cdot t}, Q_{\cdot t}, z^p_{\cdot t}, z^q_{\cdot t}, y_{\cdot t}, w_{\cdot t}, u, L^{p+}_{\cdot t}, L^{p-}_{\cdot t}, L^{q+}_{\cdot t}, L^{q-}_{\cdot t})$. Let*

- *X^1 be the set of $\{x_t \mid t = 1, \ldots, T\}$ satisfying constraints* (1b)-(1o)*;*
- *$X^1_{t'\omega}$ be the set of $\{\hat{x}_t \mid t = 1, \ldots, T\}$ such that there exists a $\{x_t \mid t = t', \ldots, T\}$ satisfying constraints in model* (2) *given $\hat{x}_{t'-1}$, for each $t' = 2, 3, \ldots$ and $\omega \in \Omega$;*
- *$X^{t\omega}$ be the set of $\{x_{\tilde{t}} \mid \tilde{t} = t, \ldots, T\}$ satisfying the constraints* (2b)-(2t)*.*
- *$X^{t\omega}_{t'\omega'}$ be the set of $\{\hat{x}_{\tilde{t}} \mid \tilde{t} = t, \ldots, T\}$ such that there exists a $\{x_{\tilde{t}} \mid \tilde{t} = t', \ldots, T\}$ satisfying constraints in model* (2) *given $\hat{x}_{t'-1}$, for all $\omega' \in \Omega$ and $t' = t + \tau^{\omega'} + 1, \ldots, T$;*

The relatively complete recourse result can be presented as:

Proposition 2. *$X^1 \subseteq \cap_{t=2,\ldots,T,\omega\in\Omega} X^1_{t\omega}$ and $X^{t\omega} \subseteq \cap_{\omega'\in\Omega, t'=t+\tau^{\omega'}+1,\ldots,T} X^{t\omega}_{t'\omega'}$.*

Proof. From Lemma 1 we know that the set $\tilde{X}^1 = \{x_t \mid s^p_{gt} \in [\underline{s}^p_g, \bar{s}^p_g], w_{bt} \in [0, \bar{I}_b], u \in [0, \bar{u}_b], \forall t = 1, \ldots, T\} \subseteq X^1_{t\omega}$ for every $t = 2, \ldots, T, \omega \in \Omega$, and given a (t, ω) pair, $\tilde{X}^{t\omega} = \{x_{\tilde{t}} \mid s^p_{gt} \in [\underline{s}^p_g, \bar{s}^p_g], w_{bt} \in [0, \bar{I}_b], u \in [0, \bar{u}_b], \tilde{t} = t, \ldots, T\} \subseteq X^{t\omega}_{t'\omega'}$ for every $\omega' \in \Omega, t' = t + \tau^{\omega'} + 1, \ldots, T$. Since there are other constraints in model (1) and (2), we can obtain $X^1 \subseteq \tilde{X}^1$ and $X^{t\omega} \subseteq \tilde{X}^{t\omega}$, which leads to the proposition (Rockafellar and Wets 1976). □

Next, we show that $f^\omega_t(\hat{s}^p_{\cdot t-1}, \hat{w}_{\cdot t-1}, \hat{u})$ is convex in $(\hat{s}^p_{\cdot t-1}, \hat{w}_{\cdot t-1}, \hat{u})$ for all $t = 2, 3, \ldots, \omega \in \Omega$.

Proposition 3. *$f^\omega_t(\hat{s}^p_{\cdot t-1}, \hat{w}_{\cdot t-1}, \hat{u})$ are convex functions of $(\hat{s}^p_{\cdot t-1}, \hat{w}_{\cdot t-1}, \hat{u})$ on the domain $\{(s^p, w, u) \mid s^p_g \in [\underline{s}^p_g, \bar{s}^p_g], \forall g \in \mathcal{G}; w_b \in [0, \bar{I}_b], u_b \in [0, \bar{u}_b], \forall b \in \mathcal{B}\}$, for all $t = 2, 3, \ldots$ and $\omega \in \Omega$.*

Proof. We prove this convexity result by induction. Suppose it is true that given a t, $f^\omega_t(\hat{s}^p_{\cdot t-1}, \hat{w}_{\cdot t-1}, \hat{u})$ is convex if for all $t' > t$, $f^\omega_{t'}(\hat{s}^p_{\cdot t'-1}, \hat{w}_{\cdot t'-1}, \hat{u})$ is convex. This holds for $t = T$. For $t' > T$, the function takes value 0 according to Assumption A.3. When $t = T$, for all $\omega \in \Omega$, model (2) has a convex objective function, containing only the linear combination of convex functions C (Assumption A.4). The feasibility region is the intersection of a polytope and second-order cones, parametrized by $\hat{s}^p_{\cdot T-1}, \hat{w}_{\cdot T-1}$ and $\hat{u}$ on the right hand side of the constraints (2r)-(2t). With a simplified notation, the dual problem of model (2) is:

$$\max_{\gamma,\eta,\zeta,\lambda} \quad \min_{x} \quad \gamma^\top \hat{s}^p_{\cdot T-1} + \eta^\top \hat{w}_{\cdot T-1} + \zeta^\top \hat{u} + \mathcal{L}(\lambda, x) \tag{6}$$

Here λ in the Lagrangian function $\mathcal{L}(\lambda, x)$ represents the dual variables for constraints (2b)-(2q) and x follows Definition 1. Slater's condition is satisfied with the solution listed in (5), which leads to strong duality, i.e., the optimal value of dual problem (6) equals to $f^\omega_T(\hat{s}^p_{\cdot T-1}, \hat{w}_{\cdot T-1}, \hat{u})$ given $\hat{s}^p_{\cdot T-1}, \hat{w}_{\cdot T-1}$ and $\hat{u}$. Lemma 1 shows that $f^\omega_T(\hat{s}^p_{\cdot T-1}, \hat{w}_{\cdot T-1}, \hat{u})$ is finite. Since the inner minimization

problem is an affine function of $\hat{s}^p_{\cdot T-1}, \hat{w}_{\cdot T-1}$ and $\hat{u}$, and the supremum of convex functions is convex, $f^\omega_T(\hat{s}^p_{\cdot T-1}, \hat{w}_{\cdot T-1}, \hat{u})$ is convex.

Now we prove that if the hypothesis holds for t, it also holds for $t-1$. The proof is similar to the case $t = T$. The only difference is that for the objective function of the dual problem (6) now contains convex functions $f^\omega_{t'}$ with $t' > t, \omega \in \Omega$, which are convex functions of x and can be merged into the term $\mathcal{L}(\lambda, x)$. The rest of the steps and the conclusion remain the same, i.e., $f^\omega_{t-1}(\hat{s}^p_{\cdot t-2}, \hat{w}_{\cdot t-2}, \hat{u})$ is convex. Thus it concludes the proof. □

3 An SDDP-based Decomposition Algorithm

We present an algorithm to solve model (1). A regular multi-stage stochastic program where uncertainty occurs in every time period can be solved by decomposition algorithms such as the SDDP algorithm (Pereira and Pinto 1991). Our problem is different in setting that a "stage" includes all decisions between two disruptions and its length is a random variable. Nevertheless, we show that a variation of the SDDP algorithm can solve our problem and cuts can be shared among value functions f^ω_t.

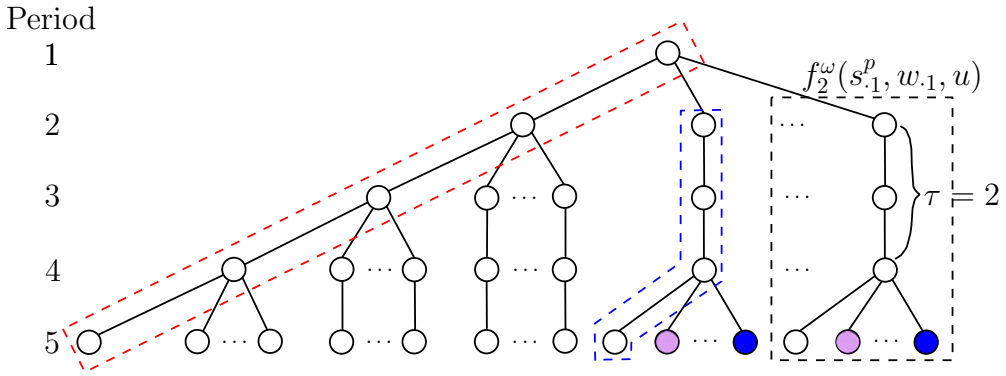

Figure 2: A scenario tree illustration of the OPF problem under stochastic $N-1$ disruptions with $T = 5$, $\tau^\omega = \tau = 2$.

To help understand the decomposition algorithm, we show a scenario tree of the OPF optimization problem in distribution networks under stochastic $N-1$ disruptions as Figure 2. Each node in this scenario tree represents the decisions at a time period along a specific scenario path. The red box of the left diagonal branch represents the decisions that is carried out if no disruption is observed, corresponding to model (1). The black box on the right corresponds to model (2) with $t_D = 2$ and some $\omega \in \Omega$, of which the value function is f^ω_2. The blue polygon box represents the decisions if a disruption occurs at time 2 and no more disruption will occur. Both purple nodes (shaded) lead to the same value function, $f^{\omega_1}_5$, while the blue nodes (solid) lead to $f^{\omega_2}_5, \omega_1 \neq \omega_2$, with the same disruption time but a different disrupted component. If we generate a lower approximation function (cut) for a purple node, it is valid for all other purple nodes in the scenario

tree, which leads to a shared cut. With this illustration in mind, we present the decomposition algorithm to solve model (1) and its convergence properties.

3.1 Decomposition Algorithm

The SDDP algorithm generates valid linear cuts iteratively to approximate value functions from below. We refer to Ding et al. (2019), Dowson and Kapelevich (2017), Shapiro (2011) for a detailed discussion about theory and implementation of SDDP. As pointed out in Dowson (2018), the SDDP algorithm's output is a set of decision rules at each time period, defined as a *policy*. A policy is essentially using the optimal solution from the approximation problem with the generated cuts, given the state of the system, as described in later parts of this section.

Since we have the relatively complete recourse property from Proposition 2, only optimality cuts need to be generated to approximate the value function f. With the convexity result in Proposition 3, we know that f can be approximated by linear cuts from below. For a specific (t_D, ω) pair, we denote the lower approximation of $f^{\omega}_{t_D}$ by $\theta^{\omega}_{t_D}$, and the l-th cuts can be written as follows:

$$\begin{aligned}\theta^{\omega}_{t_D} \geq & \hat{v}^{t_D\omega l} + \gamma^{t_D\omega l\top}(s^{p}_{\cdot t_D-1} - \hat{s}^{p,t_D\omega l}_{\cdot t_D-1}) + \eta^{t_D\omega l\top}(w_{\cdot t_D-1} - \hat{w}^{t_D\omega l}_{\cdot t_D-1}) + \\ & \zeta^{t_D\omega l\top}(u - \hat{u}^{t_D\omega l}) \qquad \forall l = 1, 2, \ldots. \end{aligned} \tag{7}$$

The cut intercept, $\hat{v}^{t_D\omega l}$, and cut gradients, $(\gamma^{t_D\omega l}, \eta^{t_D\omega l}, \zeta^{t_D\omega l})$, are obtained by solving the relaxed problems corresponding to $f^{\omega}_{t_D}$:

$$(S^{\omega}_{t_D}) \quad \min \quad \sum_{t=1}^{T}\sum_{\omega\in\Omega} p^{\omega}_{t}\left[C_{t_D,t_D+\tau^{\omega}+t-1}(s^{p}, L^{p+}, L^{p-}, L^{q+}, L^{q-}) + \theta^{\omega}_{t_D+\tau^{\omega}+t}\right] \tag{8a}$$

$$\text{s.t.} \quad (2\text{b}) - (2\text{q})$$

$$s^{p}_{gt_D-1} = \hat{s}^{p}_{gt_D-1} \qquad \forall\, g \in \mathcal{G} \tag{8b}$$

$$w_{bt_D-1} = \hat{w}_{bt_D-1} \qquad \forall\, b \in \mathcal{B} \tag{8c}$$

$$u_b = \hat{u}_b \qquad \forall\, b \in \mathcal{B}. \tag{8d}$$

$$\theta^{\omega}_{t} \geq \hat{v}^{t\omega l} + \gamma^{t\omega l\top}(s^{p}_{\cdot t-1} - \hat{s}^{p,t\omega l}_{\cdot t-1}) + \eta^{t\omega l\top}(w_{\cdot t-1} - \hat{w}^{t\omega l}_{\cdot t-1}) + \zeta^{t\omega l\top}(u - \hat{u}^{t\omega l})$$
$$\forall\, \omega \in \Omega, t \in t_D + \tau^{\omega} + 1, \ldots, T, l \in \mathcal{C}^{\omega}_{t}, \tag{8e}$$

where we denote the set of cuts for a specific f^{ω}_{t} as $\mathcal{C}^{\omega}_{t}$. The intercept, $\hat{v}^{t_D\omega l}$, equals to the optimal value of model (8) and the cut gradients, $(\gamma^{t_D\omega l}, \eta^{t_D\omega l}, \zeta^{t_D\omega l})$, are the optimal dual value of the constraints (8b)-(8d), respectively. With the lower approximation for each f^{ω}_{t} established, we can write down the lower approximation for model (1) as:

$$(M) \quad \hat{z} = \min \quad \sum_{b\in\mathcal{B}} c^{B}_{b} u_b + \sum_{t=1}^{T}\sum_{\omega\in\Omega} p^{\omega}_{t}\left[C_{1,t}(s^{p}, L^{p+}, L^{p-}, L^{q+}, L^{q-}) + \theta^{\omega}_{1+t}\right] \tag{9a}$$

s.t. (1b) − (1o)

$$\theta_t^{\omega} \geq \hat{v}^{t\omega l} + \gamma^{t\omega l\top}(s^p_{\cdot t-1} - \hat{s}^{p,t\omega l}_{\cdot t-1}) + \eta^{t\omega l\top}(w_{\cdot t-1} - \hat{w}^{t\omega l}_{\cdot t-1}) + \zeta^{t\omega l\top}(u - \hat{u}^{t\omega l})$$
$$\forall\, \omega \in \Omega, t \in 2, \ldots, T, l \in \mathcal{C}_t^{\omega}. \tag{9b}$$

Similar to the SDDP algorithm, solutions $(\hat{s}^p, \hat{w}, \hat{u})$ are obtained from sampling. However, with stochastic disruptions, we do not have to sample the uncertainty in every time period. Instead, each sample path contains information about disruptions: their occurrence time and scenario, denoted as $\mathcal{P}_n = \{(t_i, \omega_i), i = 1, \ldots, D_n\}$, where D_n denotes the number of disruptions observed in the n-th sample path. In the backward pass, we compute the cuts from $t = T$ to $t = 2$. For each sample path, the forward pass provides a trial solution, so that we can generate a lower estimation for f_t^{ω}, as long as time t satisfies some cut generation rule. An example of such rule is that given the sample path n, a cut can only be generated for f_t^{ω} if $t \notin \{t_i + 1, \ldots, t_i + \tau^{\omega_i}\}, \forall i = 1, \ldots, D_n$. Different cut generation rules are discussed in detail in Section 4.1.1. We now outline the decomposition algorithm in Algorithm 1.

For the n-th forward pass, the solutions before h-th disruption is denoted by $(\hat{s}^{p,h,n}, \hat{w}^{h,n}, \hat{u}^n)$, $h = 1, \ldots, D_n$, based on which the objective value, z_n, can be calculated. For $h = 1$, the solution corresponds to the nominal scenario where no disruption occurs throughout the time horizon (the red box in Figure 2). Algorithm 1 can be considered taking a multi-cut approach as no cuts averaging takes place (Birge and Louveaux 1988).

A major difference between our decomposition algorithm and the regular SDDP algorithm is that due to the infrequency of the disruption, in the backward pass there can be duplicate cuts if the sample paths leading to the (t, ω) are the same. For example, for a disruption problem with $T = 5, \Omega = \{1\}, \tau^1 = 1$, suppose we have two sample paths $\mathcal{P}_1 = \{(3, 1)\}$ and $\mathcal{P}_2 = \{(4, 1)\}$, then for $t = 3$, the two sample paths will obtain same $(\hat{s}^p_{\cdot t-1}, \hat{w}_{\cdot t-1}, \hat{u})$, which means the same cut will be generated. In this case, given a t in the backward pass, we can identify the distinct sample paths and only generate cuts for the trial solutions obtained by those paths, as shown in Step 22-27.

Multiple termination criteria have been discussed in previous literature, including, but not limited to, termination when the gap between the lower bound and the statistical upper bound is small enough, termination when the lower bound is within the confidence interval of the statistical upper bound, and termination at a fixed number of iterations (Pereira and Pinto 1991, Rebennack 2016, Shapiro 2011). In our case the upper bound estimation inherently has a large variance due to drastic differences between disruption scenarios, which makes the first two termination criteria ineffective; see detailed results in Section 4.2. Therefore, we terminate our algorithm after a fixed number of iterations which is large enough for the lower bound to stabilize.

Algorithm 1: SDDP-based Decomposition Algorithm

Initialize with lower bound $\underline{z} := 0$, number of sample paths N^p and iteration number $k := 1$;
repeat
  Forward pass:
  for $n = 1, 2, \ldots, N^p$ **do**
    Set $D_n := 1, t := 1, \mathcal{P}_n = \{\}$;
    while $t < T$ **do**
      Sample the next disruption time t_D and the disruption scenario ω;
      if $D_n = 1$ **then**
        Solve the master problem (M) and obtain the solution $\hat{s}^{p,D_n,n}, \hat{w}^{D_n,n}, \hat{u}^n$ and update the lower bound LB with the objective value;
      else
        With the solution $\hat{s}^{p,D_n,n}_{\cdot t-1}, \hat{w}^{D_n,n}_{\cdot t-1}, \hat{u}^n$, solve the subproblem (S^ω_t) and obtain the solution $\hat{s}^{p,D_n+1,n}, \hat{w}^{D_n+1,n}$;
      end
      Set $t := t + t_D, D_n := D_n + 1, \mathcal{P}_n := \mathcal{P}_n \cup \{(t, \omega)\}$;
    end
    Calculate the sample path cost z_n with solutions $\hat{s}^{p,D_n,n}, \hat{w}^{D_n,n}, \hat{u}^n,\ D_n = 1, 2, \ldots$;
  end
  Sample additional N' paths and calculate the statistical upper bound $\bar{z} = \frac{1}{N'} \sum_{n=1}^{N'} z_n$, the standard deviation of the upper bound estimator $\sigma_z = \sqrt{\frac{1}{N'^2} \sum_{n=1}^{N'} (\bar{z} - z_n)^2}$, and the 95% confidence interval $\mathcal{Z} = [\bar{z} - 1.96\sigma_z, \bar{z} - 1.96\sigma_z]$;
  Backward pass:
  for $t = T, T-1, \ldots, 2$ **do**
    $\mathcal{D} := \{\}, \mathcal{M} := \{\}$;
    for $n = 1, 2, \ldots, N^p$ **do**
      if *t satisfies the cut generation rule* **then**
        if $\{(t', \omega') \mid (t', \omega') \in \mathcal{P}_n, t' < t\} \notin \mathcal{D}$ **then**
          $\mathcal{D} := \mathcal{D} \cup \{(t', \omega') \mid (t', \omega') \in \mathcal{P}_n, t' < t\}$;
          $\mathcal{M} := \mathcal{M} \cup \{n\}$;
        end
      end
    end
    for $n \in \mathcal{M}$ **do**
      for $\omega \in \Omega$ **do**
        Solve the problem (S^ω_t) with solution $\hat{s}^{p,h,n}_{\cdot t-1}, \hat{w}^{h,n}_{\cdot t-1}, \hat{u}^n$, where h is the largest index of $(t', \omega') \in \mathcal{P}_n$ such that $t' < t$;
        Obtain dual solution λ, γ and μ;
        Generate a linear cutting plane (7) and append it to problem (S^ω_t);
      end
    end
  end
  Solve (M), obtain the optimal value $\hat{z}$ and update the lower bound $\underline{z} := \max\{\underline{z}, \hat{z}\}$;
  $k := k + 1$;
until *Termination criterion is met*;

3.2 Asymptotic Convergence Proof

We prove that Algorithm 1 converges asymptotically. The convergence property of the SDDP algorithm has been discussed in Girardeau et al. (2014), Linowsky and Philpott (2005), Philpott

and Guan (2008), for both linear program and convex program recourses. In addition to Assumptions A.1-A.4, we list the rest of assumptions on Algorithm 1 as follows:

A.6 Suppose the collection of all possible forward paths is $\mathbb{P}$, and the forward paths obtained in iteration k in Algorithm 1 are denoted as $\mathcal{P}_n^k, n = 1, \ldots, N$. When $k \to \infty$,

$$\left|\{\mathcal{P}_n^k \mid \mathcal{P}_n^k = \mathcal{P}, n = 1, \ldots, N\}\right| = \infty$$

with probability 1 for every $\mathcal{P} \in \mathbb{P}$.

A.7 For any infinite subsequence $J \subseteq \mathbb{N}$,

$$\left|(k, n) \mid (t, \omega) \in \mathcal{P}_n^k, k \in J, n = 1, \ldots, N\right| = \infty$$

with probability 1 for all $t = 2, \ldots, T, \omega \in \Omega$.

A.8 Variables $L^{p+}, L^{p-}, L^{q+}, L^{q-}$ have finite upper bounds.

A.9 The cut coefficients, $\gamma^{t\omega l}, \eta^{t\omega l}, \zeta^{t\omega l}$, are all finite in every iteration $l \in \mathcal{C}_t^\omega$ for every $t = 2, \ldots, T, \omega \in \Omega$.

Assumption A.6 is equivalent to the *Forward Pass Sampling Property* and Assumption A.7 is equivalent to the *Backward Pass Sampling Property* in Philpott and Guan (2008). If the algorithm never terminates, Assumption A.6 indicates that any forward path is traversed infinitely many times with probability 1, and Assumption A.7 implies that each f_t^ω goes through the backward pass infinite times with infinitely many cuts generated. It is not optimal to have both L^{p+} and L^{p-} positive (same for L^{q+} and L^{q-}), and all other variables in constraints (1b)-(1c) and constraints (2b)-(2c) are bounded. Therefore, we can derive the upper bounds $L^{p+}, L^{p-}, L^{q+}, L^{q-}$ from the bounds on z^p, z^q, s^p, s^q, P and Q as stated in Assumption A.8. Assumption A.9 naturally holds for the interior of the domain because f_t^ω is convex and bounded. We require that the dual values are finite for the boundary points: if we consider the optimal dual solution is a convex combination of sets of dual extreme points and dual extreme rays, we can always set the coefficients for the rays to be zero and yield an optimal dual value that is also finite. This requirement is equivalent to the Assumption 6(a) in Girardeau et al. (2014).

We prove the asymptotic convergence for the SDDP-based algorithm, even when the number of stages and the stage lengths are both random variables. We start with the validity proof of cuts. Each subproblem (S_t^ω) is essentially a function of the solution, $(\hat{s}_{\cdot t-1}^p, \hat{w}_{\cdot t-1}, \hat{u})$, which we denote as $f_t^{\omega,k}(\hat{s}_{\cdot t-1}^{p,k}, \hat{w}_{\cdot t-1}^k, \hat{u}^k)$ when it is solved for the k-th time.

Lemma 4. *Every cut generated in Algorithm 1, in the form of* (7)*, is a valid lower approximation for the corresponding f_t^ω for all $t \in \{2, \ldots, T\}, \omega \in \Omega$.*

Proof. Suppose given a t, for all $t' > t$, the generated cuts are lower approximation for $f_{t'}^{\omega}, \forall \omega \in \Omega$, then the cuts generated for f_t^{ω} are valid lower approximation. First we prove that for $t = T$, the cut is a valid lower bound, since f_T^{ω} is a convex function as shown in Proposition 3, and the generated cuts are simply its subgradients.

We want to prove for $t-1$ the hypothesis holds if it is true for time t. From the hypothesis we know that for all $t' \geq t, \omega \in \Omega$, the l-th cut $\hat{v}^{t'\omega l} + \gamma^{t'\omega l^{\top}}(s^p_{\cdot t'-1} - \hat{s}^{p,t'\omega l}_{\cdot t'-1}) + \eta^{t'\omega l^{\top}}(w_{\cdot t'-1} - \hat{w}^{t'\omega l}_{\cdot t'-1}) + \zeta^{t'\omega l^{\top}}(u - \hat{u}^{t'\omega l}) \leq f_{t'}^{\omega}(s^p_{\cdot t'-1}, w_{\cdot t'-1}, u)$ for all feasible $(s^p_{t'-1}, w_{t'-1}, u)$, which leads to $f_{t-1}^{\omega,l}(s^p_{\cdot t-2}, w_{\cdot t-2}, u) \leq f_{t-1}^{\omega}(s^p_{\cdot t-2}, w_{\cdot t-2}, u)$ for all feasible (s^p_{t-2}, w_{t-2}, u) (see Corollary 2 in Rebennack 2016). The $l+1$-th cut is the lower approximation of $f_{t-1}^{\omega,l}$, and it automatically guarantees that it is also a valid lower approximation of f_{t-1}^{ω}. This shows the hypothesis for $t-1$ is also true. By backward induction we can conclude the proof. □

We prove the asymptotic convergence of Algorithm 1 with the following theorems.

Theorem 5. *Suppose that Assumptions A.1-A.9 hold for any given t, $1 \leq t \leq T$, $\omega \in \Omega$ and any given infinite set $K \subseteq \mathbb{N}$, and that the sequence $\{(s^{p,k}_{\cdot t-1}, w^k_{\cdot t-1}, u^k)\}_{k\in K}$ generated by Algorithm 1 converges to some given vector $(s^{p,0}_{\cdot t-1}, w^0_{\cdot t-1}, u^0)$. Then there exists an infinite set $J \subseteq K$ such that:*

1. *the sequence $\{\mathcal{X}_t^{\omega,k}\}_{k\in J}$ converges to some vector $\mathcal{X}_t^{\omega,0}$, where $\mathcal{X}_t = \{x_{t'} \mid t' = t, \ldots, T\}$ represents the collection of decisions stated in Definition 1.*
2. *the sequence $\{f_t^{\omega,k}(s^{p,k}_{\cdot t-1}, w^k_{\cdot t-1}, u^k)\}_{k\in J}$ converges to $f_t^{\omega}(s^{p,0}_{\cdot t-1}, w^0_{\cdot t-1}, u^0)$ w.p.1.*
3. *the sequence $\{\theta_t^{\omega,k}\}_{k\in J}$ converges to $f_t^{\omega}(s^{p,0}_{\cdot t-1}, w^0_{\cdot t-1}, u^0)$ w.p.1.*

Proof. The proof largely follows the proofs for Lemma 4.1 and 4.2 from Linowsky and Philpott (2005). Notice that Assumption A.6 and A.7 handle the sampling independence issue listed in Girardeau et al. (2014), given Assumption A.1 and finite sets $\mathcal{T}$ and Ω.

We prove the theorem by backward induction. For $t = T$, by model (2) and Assumption A.8, the primal feasible set is bounded for every f_T^{ω}. From the Bolzano-Weierstrass Theorem, we know that for every infinite sequence in a bounded set there has to be a convergent subsequence. We denote such subsequence as J and its limit as $x_T^{\omega,0}$. Also, for $t = T, \omega \in \Omega$, $f_T^{\omega,k}(s^{p,k}_{\cdot T-1}, w^k_{\cdot T-1}, u^k) = f_T^{\omega}(s^{p,k}_{\cdot T-1}, w^k_{\cdot T-1}, u^k)$ since all θ terms are just zeros, and its limit converges to $f_T^{\omega}(s^{p,0}_{\cdot T-1}, w^0_{\cdot T-1}, u^0)$ as it is continuous.

From Lemma 4, for $k \in J$ we have:

$$\begin{aligned} f_T^{\omega}(s^{p,k}_{\cdot T-1}, w^k_{\cdot T-1}, u^k) \geq \theta_T^{\omega,k} &\geq f_T^{\omega,k-1}(s^{p,k-1}_{\cdot T-1}, w^{k-1}_{\cdot T-1}, u^{k-1}) + \gamma^{T\omega k-1^{\top}}(s^{p,k}_{\cdot T-1} - s^{p,k-1}_{\cdot T-1}) + \\ &\quad \eta^{T\omega k-1^{\top}}(w^k_{\cdot T-1} - w^{k-1}_{\cdot T-1}) + \zeta^{T\omega k-1^{\top}}(u^k - u^{k-1}) \\ &= f_T^{\omega,k-1}(s^{p,k-1}_{\cdot T-1}, w^{k-1}_{\cdot T-1}, u^{k-1}) + \Delta_T^{\omega,k} \end{aligned}$$

with

$$\Delta_T^{\omega,k} = \lambda^{T\omega k-1\top}(s_{\cdot T-1}^{p,k} - s_{\cdot T-1}^{p,k-1}) + \gamma^{T\omega k-1\top}(w_{\cdot T-1}^{k} - w_{\cdot T-1}^{k-1}) + \mu^{T\omega k-1\top}(u^k - u^{k-1}).$$

We subtract $f_T^{\omega}(s_{\cdot T-1}^{p,k}, w_{\cdot T-1}^{k}, u^k)$ from the inequality and take the absolute value:

$$\begin{aligned}\left|\theta_T^{\omega,k} - f_T^{\omega}(s_{\cdot T-1}^{p,k}, w_{\cdot T-1}^{k}, u^k)\right| &\leq \left|f_T^{\omega,k-1}(s_{\cdot T-1}^{p,k-1}, w_{\cdot T-1}^{k-1}, u^{k-1}) - f_T^{\omega}(s_{\cdot T-1}^{p,k}, w_{\cdot T-1}^{k}, u^k) + \Delta_T^{\omega,k}\right| \\ &\leq \left|f_T^{\omega,k-1}(s_{\cdot T-1}^{p,k-1}, w_{\cdot T-1}^{k-1}, u^{k-1}) - f_T^{\omega}(s_{\cdot T-1}^{p,k}, w_{\cdot T-1}^{k}, u^k)\right| + \left|\Delta_T^{\omega,k}\right| \\ &= \left|f_T^{\omega}(s_{\cdot T-1}^{p,k-1}, w_{\cdot T-1}^{k-1}, u^{k-1}) - f_T^{\omega}(s_{\cdot T-1}^{p,k}, w_{\cdot T-1}^{k}, u^k)\right| + \left|\Delta_T^{\omega,k}\right|.\end{aligned}$$

Due to continuity of the functions f_t^{ω}, we have:

$$\lim_{k\to\infty}\left|f_T^{\omega}(s_{\cdot T-1}^{p,k-1}, w_{\cdot T-1}^{k-1}, u^{k-1}) - f_T^{\omega}(s_{\cdot T-1}^{p,k}, w_{\cdot T-1}^{k}, u^k)\right| = 0,$$

as the solution sequence converges to a point $(s_{\cdot T-1}^{p,0}, w_{\cdot T-1}^{0}, u^0)$. We also have

$$\lim_{k\to\infty}\left|\Delta_T^{\omega,k}\right| = 0,$$

as the dual values are finite, stated in Assumption A.9, and the sequence $(s_{\cdot T-1}^{p,k}, w_{\cdot T-1}^{k}, u^k)$ converges. We can further derive the relationship between $\theta_T^{\omega,k}$ and $f_T^{\omega}(s_{\cdot T-1}^{p,0}, w_{\cdot T-1}^{0}, u^0)$ by:

$$\begin{aligned}\left|\theta_T^{\omega,k} - f_T^{\omega}(s_{\cdot T-1}^{p,0}, w_{\cdot T-1}^{0}, u^0)\right| \leq \left|\theta_T^{\omega,k} - f_T^{\omega}(s_{\cdot T-1}^{p,k}, w_{\cdot T-1}^{k}, u^k)\right| + \\ \left|f_T^{\omega}(s_{\cdot T-1}^{p,k}, w_{\cdot T-1}^{k}, u^k) - f_T^{\omega}(s_{\cdot T-1}^{p,0}, w_{\cdot T-1}^{0}, u^0)\right| \to 0 \text{ as } k\to\infty,\end{aligned}$$

which concludes the proof for $t = T$.

Suppose the theorem holds for all $t' \geq t$, we want to prove that the hypothesis also holds for $t-1$. Similarly, since the primal feasible set is bounded, there exists an infinite subsequence of $J' \subseteq \mathbb{N}$ such that $\{\mathcal{X}_{t-1}^{\omega,k}\}_{k\in J'}$ converges to some $\mathcal{X}_{t-1}^{\omega,0}$. According to Assumption A.7, we can obtain an infinite subsequence $J_{t'}^{\omega'} \subseteq J', t' = t+\tau^{\omega}, \ldots, T, \omega' \in \Omega$, where $(t',\omega') \in \mathcal{P}_n^k$ for every $k \in J_{t'}^{\omega'}$ and some $n = 1, 2, \ldots, N^p$. Since the sequence $J = \cup_{t'=t+\tau^{\omega},\ldots,T,\omega'\in\Omega} J_{t'}^{\omega'}$ is an infinite sequence in a bounded set, $\{\mathcal{X}_{t-1}^{\omega,k}\}_{k\in J} \to \mathcal{X}_{t-1}^{\omega,0}$.

We can derive that the convergence of the approximation function $f_{t-1}^{\omega,k}(s_{\cdot t-2}^{p,k}, w_{\cdot t-2}^{k}, u^k)$:

$$\begin{aligned}&f_{t-1}^{\omega}(s_{\cdot t-2}^{p,k}, w_{\cdot t-2}^{k}, u^k) \geq f_{t-1}^{\omega,k}(s_{\cdot t-2}^{p,k}, w_{\cdot t-2}^{k}, u^k) \\ &= f_{t-1}^{\omega}(s_{\cdot t-2}^{p,k}, w_{\cdot t-2}^{k}, u^k) + \sum_{t'=1}^{T}\sum_{\omega'\in\Omega} p_{t'}^{\omega'}\left[\theta_{t+\tau^{\omega}+t'}^{\omega',k} - f_{t+\tau^{\omega}+t'}^{\omega'}(s_{\cdot t+\tau^{\omega}+t'-1}^{p,k}, w_{\cdot t+\tau^{\omega}+t'-1}^{k}, u^k)\right]\end{aligned}$$

Therefore, we can obtain the absolute value of the difference between the approximation and the actual functions:

$$\left|f_{t-1}^{\omega,k}(s_{\cdot t-2}^{p,k}, w_{\cdot t-2}^{k}, u^k) - f_{t-1}^{\omega}(s_{\cdot t-2}^{p,k}, w_{\cdot t-2}^{k}, u^k)\right| \leq \sum_{t'=1}^{T}\sum_{\omega'\in\Omega} p_{t'}^{\omega'}\left|\theta_{t+\tau^{\omega}+t'}^{\omega',k} -\right.$$

$$f^{\omega'}_{t+\tau^\omega+t'}(s^{p,k}_{\cdot t+\tau^\omega+t'-1}, w^k_{\cdot t+\tau^\omega+t'-1}, u^k)\Big|,$$

the right-hand side of which converges to 0 w.p.1 as $k \to \infty$ according to the hypothesis and the selection of sequence J. With the continuity of f^ω_{t-1} and the convergence of $(s^{p,k}_{\cdot t-2}, w^k_{\cdot t-2}, u^k)$ to $(s^{p,0}_{\cdot t-2}, w^0_{\cdot t-2}, u^0)$:

$$\left|f^{\omega,k}_{t-1}(s^{p,k}_{\cdot t-2}, w^k_{\cdot t-2}, u^k) - f^\omega_{t-1}(s^{p,0}_{\cdot t-2}, w^0_{\cdot t-2}, u^0)\right| \leq \left|f^\omega_{t-1}(s^{p,k}_{\cdot t-2}, w^k_{\cdot t-2}, u^k) - f^\omega_{t-1}(s^{p,0}_{\cdot t-2}, w^0_{\cdot t-2}, u^0)\right|,$$

both terms of the right-hand side converge to 0 w.p.1 as $k \to +\infty$. This proves the second part of the theorem for time period $t-1$.

For the last part of the proof, we have the inequalities similar to the $t = T$ case:

$$f^\omega_{t-1}(s^{p,k}_{t-2}, w^k_{t-2}, u^k) \geq \theta^{\omega,k}_{t-1} \geq f^{\omega,k-1}_{t-1}(s^{p,k-1}_{t-2}, w^{k-1}_{t-2}, u^{k-1}) + \Delta^{\omega,k}_{t-1},$$

with

$$\Delta^{\omega,k}_{t-1} = \gamma^{t-1\omega k-1\top}(s^{p,k}_{\cdot t-2} - s^{p,k-1}_{\cdot t-2}) + \eta^{t-1\omega k-1\top}(w^k_{\cdot t-2} - w^{k-1}_{\cdot t-2}) + \zeta^{t-1\omega k-1\top}(u^k - u^{k-1})$$

We can rewrite the inequality as:

$$\begin{aligned}
&\left|\theta^{\omega,k}_{t-1} - f^\omega_{t-1}(s^{p,k}_{\cdot t-2}, w^k_{\cdot t-2}, u^k)\right| \\
&\leq \left|f^{\omega,k-1}_{t-1}(s^{p,k-1}_{\cdot t-2}, w^{k-1}_{\cdot t-2}, u^{k-1}) - f^\omega_{t-1}(s^{p,k}_{\cdot t-2}, w^k_{\cdot t-2}, u^k) + \Delta^{\omega,k}_{t-1}\right| \\
&\leq \left|f^{\omega,k-1}_{t-1}(s^{p,k-1}_{\cdot t-2}, w^{k-1}_{\cdot t-2}, u^{k-1}) - f^\omega_{t-1}(s^{p,k}_{\cdot t-2}, w^k_{\cdot t-2}, u^k)\right| + \left|\Delta^{\omega,k}_{t-1}\right| \\
&\leq \left|f^{\omega,k-1}_{t-1}(s^{p,k-1}_{\cdot t-2}, w^{k-1}_{\cdot t-2}, u^{k-1}) - f^\omega_{t-1}(s^{p,0}_{\cdot t-2}, w^0_{\cdot t-2}, u^0)\right| + \left|\Delta^{\omega,k}_{t-1}\right| + \\
&\qquad \left|f^\omega_{t-1}(s^{p,0}_{\cdot t-2}, w^0_{\cdot t-2}, u^0) - f^\omega_{t-1}(s^{p,k}_{\cdot t-2}, w^k_{\cdot t-2}, u^k)\right|
\end{aligned}$$

For $k \in J$, we have the limiting results as:

$$\lim_{k\to+\infty} \left|f^{\omega,k-1}_{t-1}(s^{p,k-1}_{\cdot t-2}, w^{k-1}_{\cdot t-2}, u^{k-1}) - f^\omega_{t-1}(s^{p,0}_{\cdot t-2}, w^0_{\cdot t-2}, u^0)\right| = 0, \text{ w.p.1} \tag{10}$$

$$\lim_{k\to+\infty} \left|\Delta^{\omega,k}_{t-1}\right| = 0 \tag{11}$$

$$\lim_{k\to+\infty} \left|f^\omega_{t-1}(s^{p,0}_{\cdot t-2}, w^0_{\cdot t-2}, u^0) - f^\omega_{t-1}(s^{p,k}_{\cdot t-2}, w^k_{\cdot t-2}, u^k)\right| = 0 \tag{12}$$

Equation (10) has already been proved. Equation (11) is true since the dual values are finite and the sequence of solutions is converging. Equation (12) holds because of the continuity of function f^ω_{t-1}. Therefore,

$$\left|\theta^{\omega,k}_{t-1} - f^\omega_{t-1}(s^{p,k}_{\cdot t-2}, w^k_{\cdot t-2}, u^k)\right| \to 0 \qquad \text{as } k \to +\infty, \text{ w.p.1.}$$

Once more, we use the continuity of function f^ω_{t-1} and obtain:

$$\left|\theta^{\omega,k}_{t-1} - f^\omega_{t-1}(s^{p,0}_{\cdot t-2}, w^0_{\cdot t-2}, u^0)\right|$$

$$\leq \left|\theta_{t-1}^{\omega,k} - f_{t-1}^{\omega}(s_{\cdot t-2}^{p,k}, w_{\cdot t-2}^{k}, u^{k})\right| + \left|f_{t-1}^{\omega}(s_{\cdot t-2}^{p,k}, w_{\cdot t-2}^{k}, u^{k}) - f_{t-1}^{\omega}(s_{\cdot t-2}^{p,0}, w_{\cdot t-2}^{0}, u^{0})\right|$$
$$\to 0 \qquad \text{as } k \to +\infty \text{ w.p.1.}$$

As we finish the proof for time $t-1$, we can conclude the proof by backward induction. □

Theorem 6. *Suppose that Assumptions A.1-A.9 hold and the problem (M) solved in the k-th iteration is denoted as (M^k), the sequence of the optimal value of (M^k), $\{\hat{z}^k\}_{k\in\mathbb{N}}$, converges to z^* w.p.1, and any accumulation point of the sequence of the solution to (M^k) is an optimal solution.*

Proof. We can consider the first-stage problems taking in some dummy constant input, which automatically converges and matches the condition of Theorem 5, same as the proof in Chen and Powell (1999), Linowsky and Philpott (2005). The proof for the optimal value convergence follows the same principles as the second part of the proof for Theorem 5. Since every iteration some constraints are added to (M^k), the sequence $\{\hat{z}^k\}_{k\in\mathbb{N}}$ is nondecreasing. If a monotone sequence has a convergent subsequence that converges to some value, then the whole sequence must converge to the same value. Thus, $\{\hat{z}^k\}_{k\in\mathbb{N}}$ converges to z^*.

Given a subsequence $K \subseteq \mathbb{N}$ such that $\{\mathcal{X}_1^k\}_{k\in K}$ converges to some $\mathcal{X}_1^0$. With the results from Theorem 5, we know that there exists a subsequence $J \subseteq K$ such that:

$$\{f_t^{\omega,k}(s_{\cdot t-1}^{p,k}, w_{\cdot t-1}^{k}, u^{k})\}_{k\in J} \to f_t^{\omega}(s_{\cdot t-1}^{p,0}, w_{\cdot t-1}^{0}, u^{0}) \quad \text{w.p.1.} \quad \forall t = 2,\ldots,T, \omega \in \Omega$$

Since $\mathcal{X}_1^k$ is a feasible solution to (M), and the feasible region of (M) is bounded, as shown by Assumption A.8 and other bounds in model (1), the accumulation point $\mathcal{X}_1^0$ must be a feasible solution as well. On the other hand, we have:

$$\hat{z}^k = \sum_{b\in\mathcal{B}} c_b^B u_b^k + \sum_{t=1}^{T}\sum_{\omega\in\Omega} p_t^{\omega}\left[C_{1,t}(s^{p,k}, L^{p+,k}, L^{p-,k}, L^{q+,k}, L^{q-,k}) + \theta_{1+t}^{\omega}\right] \tag{13a}$$

$$z^* = \lim_{k\in K}\hat{z}^k = \sum_{b\in\mathcal{B}} c_b^B u_b^0 + \sum_{t=1}^{T}\sum_{\omega\in\Omega} p_t^{\omega}\left[C_{1,t}(s^{p,0}, L^{p+,0}, L^{p-,0}, L^{q+,0}, L^{q-,0}) + f_{1+t}^{\omega}(s_{\cdot,t}^{p,0}, w_{\cdot,t}^{0}, u^{0})\right] \tag{13b}$$

The equation (13b) is derived by taking limit on both sides of the equation (13a), which is the definition of $\hat{z}^k$ in model (9). This shows that the solution $\mathcal{X}_1^0$ is optimal. □

Although this asymptotic convergence proof is constructed with specifications of the distribution network optimization power flow model, it works for the general framework of optimization with stochastic disruptions with Assumptions A.1-A.9 satisfied, which are typical setups in a multi-stage stochastic program.

4 Experimental Results

In this section we show the computational efficiency of our decomposition algorithm with potential enhancements (Section 4.1), the value of the stochastic policy compared to the deterministic alternative (Section 4.2), and analysis on operational insights of distributions networks (Section 4.3). We use IEEE test cases with 13, 33 and 123 buses (Baran and Wu 1989, Schneider et al. 2018) and we refer to these by the number of buses (e.g., Case 13). We have detailed descriptions of problem setups and parameters in Online Supplement A.

Each time period, Δt, is 15 minutes as it is the typical time scale at which an off-grid microgrid is operated (Cardoso et al. 2019, Chalil Madathil et al. 2018, Grid Integration Group 2020, Mashayekh et al. 2017). We assume that p_t, defined in Assumption A.1, follows a discretized exponential distribution with a rate parameter, λ_D:

$$p_t = e^{-\lambda_D(t-1)} - e^{-\lambda_D t}, \quad t = 1, 2, \ldots, T-1 \qquad\qquad p_T = 1 - \sum_{t=1}^{T-1} p_t. \tag{14}$$

All electrical components (lines and generators) can be disrupted with equal probability ($p^\omega = \frac{1}{|\Omega|}$), and for simplicity purposes, all disruptions have the same recovery time $\tau^\omega = \tau, \forall\, \omega \in \Omega$. Our focus lies in the modeling for stochastic disruptions and the value of our stochastic policy, rather than a detailed probabilistic component failure model.

All models are constructed using JuMP package v0.18.0 (Dunning et al. 2017) in Julia v0.6.4. The convex quadratic programs are solved by Gurobi 8.1.1 (Gurobi Optimization, Inc. 2016). All tests are run on the Northwestern University server utilizing 20 Intel Xeon cores at 2.4 GHz and 120 GB of RAM. We develop the implementation of Algorithm 1 in parallelization: the forward pass is simulated and solved in parallel, while for each t iterate in the backward pass, we solve the model (2) with different scenarios ω in parallel.

We encountered numerical issues in obtaining accurate dual values using off-the-shelf-solvers (Gurobi and Ipopt). Hence we analytically derive the dual of model (2) as in Online Supplement B and directly solve it to obtain correct gradient information for cuts (7).

4.1 Computational Performance

First, we test the run-time of Algorithm 1 and the effect of cut generation enhancements and algorithm parameters. We set $T = 96$, $\tau = 16$, and $\lambda_D = \frac{1}{24}$ for all following tests in this section. Since the statistical upper bound is not used as a termination criterion, the reported computational time does not include the time executing Step 17 in Algorithm 1.

4.1.1 Improved Cut Generation Process

In a regular SDDP algorithm, cuts are generated at every stage where uncertainty occurs. Equivalently for our case, cuts can be generated for a (t, ω) pair when $(t, \omega') \in \mathcal{P}_n$ for some $\omega' \in \Omega$; in

other words, cuts are generated for (t, ω) when a disruption occurs at time t in the sample path $\mathcal{P}_n$. However, given a sample path, we can generate cuts for a (t, ω) pair as long as t is not within the recovery time of some disruptions. We denote the first rule as "DOnly" since cuts are generated only at a disruption time, while we denote the second rule as "GenAll" as all possible cuts are generated. We set the number of sample paths used in each iteration to $N^p = 5$ and terminate Algorithm 1 after 20 iterations for GenAll and 100 iterations for DOnly to achieve a reasonable run-time and obtain sufficient observations about the algorithm's behavior.

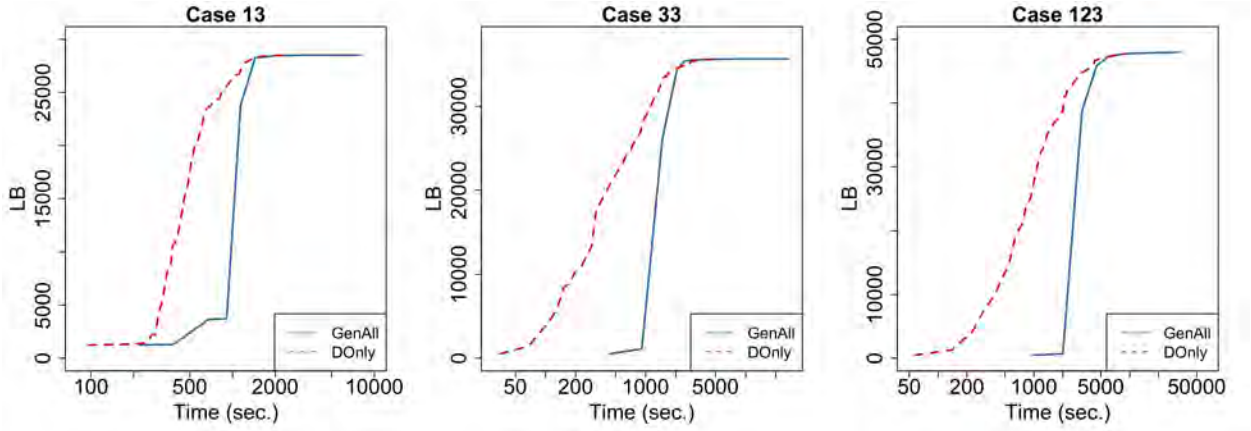

Figure 3: Lower bounds vs. run-times for cut generation rules, GenAll and DOnly.

Figure 3 shows the trend of lower bound and total run-time for the two cut generation rules. Since GenAll generates cuts for all possible (t, ω) pairs, the lower bound converges in fewer iterations, but each iteration takes longer since we need to solve more optimization problems to generate cuts. We observe that the lower bound of GenAll grows within 1% of the final lower bound after the first 10 iterations. On the other hand, it takes DOnly all 100 iterations to achieve a lower bound smaller than the lower bound obtained by GenAll in 10 iterations. Considering the overall performance that the lower bound difference is less than 1%, but the run-time of GenAll for 10 iterations is at least 20% longer than that of DOnly for 100 iterations, as shown in Table 1, we use DOnly as the cut generation rule in Algorithm 1 and it applies to all the remaining tests in the paper.

Test Case	GenAll		DOnly	
	LB ($)	Time (sec.)	*LB* ($)	Time (sec.)
Case 13	28494.4	2703.6	28487.2	2279.8
Case 33	35636.2	6058.2	35599.3	4905.9
Case 123	47869.1	15807.1	47728.5	8895.0

Table 1: Lower bounds and total run-times after 10 iterations for GenAll and 100 iterations for DOnly.

We also pre-generate tight cuts for later stage value functions before Algorithm 1 starts. It

helps achieve a better lower bound with a small budget limit. Details of the cut pre-generating process and computational results are listed in Online Supplement C.

4.1.2 Time Performance vs. Number of Sample Paths (N^p)

The number of samples generated in each iteration, N^p, can affect the run-time of Algorithm 1: when N^p is small, cuts improve approximation for f_t^ω only for a limited decision space and convergence takes more iterations; when N^p is large, additional cuts for earlier disruptions may not provide much value for the approximation but may slow down each subsequent iterations. Here we test how the lower bound and the run-time change for various values of N^p.

We set a sampling budget limit as 500 so that the lower bound stabilizes when Algorithm 1 terminates. For example, if $N^p = 5$, Algorithm 1 terminates after 100 iterations. We present lower bounds and the run-time against the number of iterations in Figure 4 and a summary of total run-time for different N^p in Table 2. Figure 4 shows that as N^p increases, the run-time required to achieve a similar level of the lower bound first decreases and then increases for all three test cases. This confirms that there is a trade-off between the number of iterations and the quality of cuts. With a fixed budget of 500 samples, $N^p = 5$ and $N^p = 10$ are comparable as they both converge to a stable lower bound with the shortest run-time among all tested N^p. We select $N^p = 5$ for the remaining tests.

Test Case \ N^p		1	5	10	15	20
Case 13	LB ($)	28491.5	28489.4	28489.9	28491.2	28490.2
	Time (sec.)	5134.7	2875.0	3118.0	3315.2	3477.9
Case 33	LB ($)	35599.5	35608.0	35601.2	35601.9	35598.1
	Time (sec.)	11742.1	6261.5	5885.8	7346.6	7373.0
Case 123	LB ($)	47790.6	47788.3	47789.4	47758.2	47757.8
	Time (sec.)	27898.2	11434.0	11969.6	12336.7	10930.0

Table 2: Lower bounds and total run-times for $N^p = 1, 5, 10, 15, 20$ using 500 samples. Here the numbers of iterations are $500, 100, 50, 33, 25$, respectively.

4.2 Properties of the Stochastic Programming Strategy

We compare our stochastic policy obtained from Algorithm 1 with a deterministic policy that is agnostic to disruptions. The deterministic policy starts with solving an optimization model for the entire time horizon, assuming no disruption would occur. For a given sample path, once a disruption occurs, another deterministic optimization model is solved for the rest of time horizon assuming that there is no further disruption after the recovery. This procedure is repeated until we reach the end of time horizon. We evaluate both policies with 1000 identical sample paths and obtain their mean costs in an *out-of-sample* test, as the sample paths used for evaluation are not

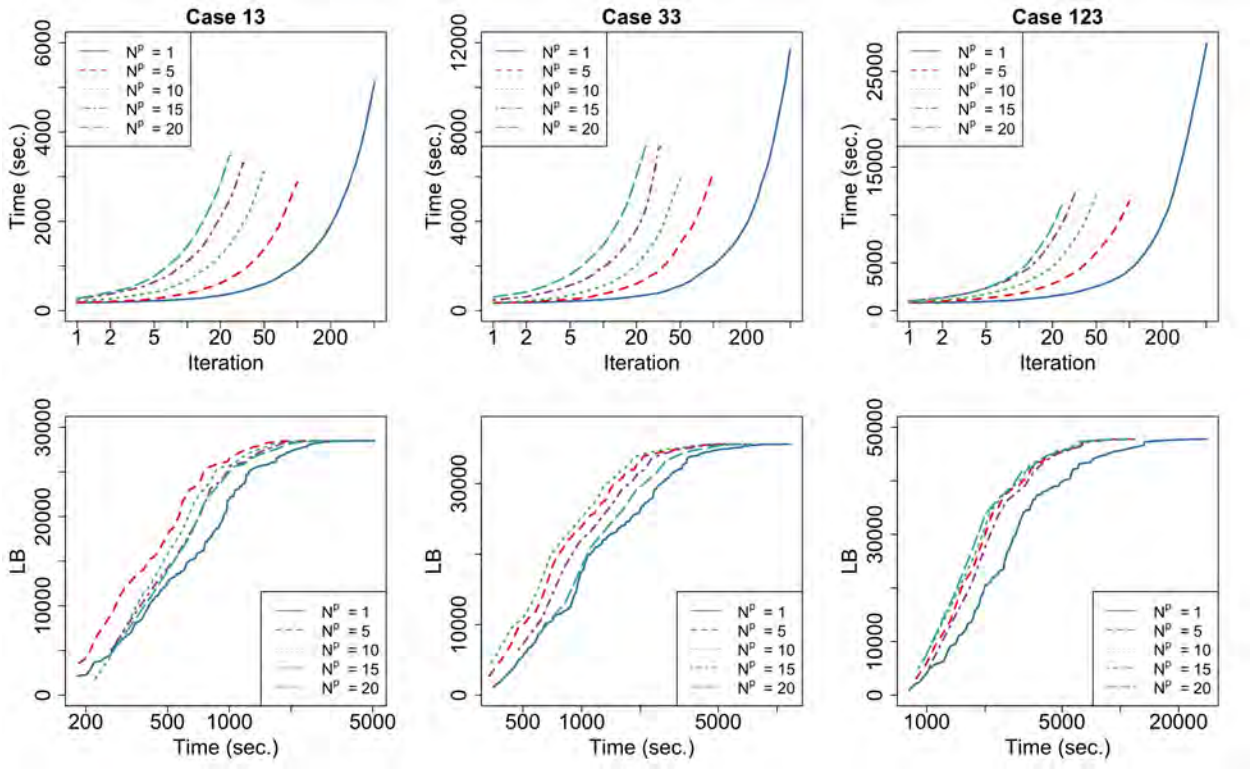

Figure 4: Run-times vs. the number of iterations and lower bounds vs. run-times for $N^p = 1, 5, 10, 15, 20$ using 500 samples. Here the numbers of iterations are $500, 100, 50, 33, 25$, respectively.

seen in the policy training.

We also present the objective values from both policies for a sample path without disruption, denoted as "Nominal". Without a disruption, the deterministic policy yields the optimal cost, while the cost of the stochastic policy is supposed to be higher because it hedges against potential disruptions. The difference between the optimal objective values between the two policies provides an estimation for the cost of incorporating uncertainty.

We set $T \in \{24, 36, 48, 72, 96\}$, $\tau = \frac{T}{6}$, and $\lambda_D = \frac{4}{T}$, which keeps the expected number of disruptions similar for different lengths of time horizon. Algorithm 1 is computed for 100 iterations with parameter $N^p = 5$. Table 3 shows the cost comparison. When no disruption occurs, the stochastic policy cost is moderately larger, as the stochastic policy-based solution usually generates more from the conventional generators and installs more battery capacity in preparation for disruptions. It is worth the increased cost when the disruption is a possibility, as we observe a saving in costs *larger than 70%* in all out-of-sample test cases by the stochastic policy. The result shows that the stochastic policy prevents the more expensive power mismatch and justifies the stochastic policy's value.

The obtained stochastic policy depends on the training samples, which is random and may lead

Test Case \ T			24	36	48	72	96
Case 13	Out-of-sample	D ($)	28994.4	38593.7	57487.1	78839.8	102282.2
		S ($)	4907.8	5763.0	11395.9	17763.9	25649.6
	Nominal	D ($)	1905.0	2011.0	2391.0	2886.0	4007.0
		S ($)	2503.2	2660.4	3101.2	3595.7	4668.7
Case 33	Out-of-sample	D ($)	51003.4	62227.2	81172.1	118222.4	156967.5
		S ($)	9630.1	11999.1	17209.8	26977.1	37423.7
	Nominal	D ($)	513.0	769.0	1033.0	1523.0	2033.0
		S ($)	814.7	1174.4	1540.1	2206.4	2908.9
Case 123	Out-of-sample	D ($)	53847.8	69273.6	95499.4	131228.3	166469.8
		S ($)	14088.8	18134.7	26017.8	38024.7	49866.4
	Nominal	D ($)	470.0	699.0	926.0	1386.0	1850.0
		S ($)	825.3	1200.0	1554.3	2290.5	3054.5

Table 3: Out-of-sample and nominal evaluations obtained for the deterministic and the stochastic policy. A sample size of 1000 is used for the out-of-sample tests. Here "D" and "S" stand for "deterministic" and "stochastic" policies, respectively.

to different lower bounds and the out-of-sample evaluations in multiple replications. We inspect how variable the lower bound and the out-of-sample evaluation of the trained policy are. The following result shows how consistent the policy is when we terminate with a fixed number of iterations. We obtain policies by repeating Algorithm 1 with 20 replications of 5000 sample paths, obtain their corresponding lower bound (LB) and obtain the mean evaluation of those policies, $\bar{z}_{5000}$. We obtain a 95% confidence interval of the policy evaluation for both LB and $\bar{z}_{5000}$ and report them in Table 4.

Test Case \ T		24	36	48	72	96
Case 13	LB ($)	5215.4 ± 2.2	5849.3 ± 4.8	12295.4 ± 4.0	18391.3 ± 5.2	28487.4 ± 10.7
	$\bar{z}_{5000}$ ($)	5184.7 ± 4.0	5970.2 ± 4.7	12819.5 ± 10.1	18102.6 ± 8.3	30097.7 ± 10.7
Case 33	LB ($)	10048.5 ± 4.9	13803.4 ± 8.7	18563.2 ± 8.9	26917.9 ± 6.6	35598.6 ± 38.1
	$\bar{z}_{5000}$ ($)	10601.7 ± 5.9	13534.9 ± 7.2	18062.0 ± 8.5	25913.5 ± 15.1	35966.2 ± 14.4
Case 123	LB ($)	13645.7 ± 6.1	19185.1 ± 7.9	24733.7 ± 14.8	36322.9 ± 17.5	47799.4 ± 46.0
	$\bar{z}_{5000}$ ($)	13535.6 ± 8.9	19838.8 ± 10.3	24874.1 ± 10.4	35943.8 ± 19.3	46411.1 ± 26.6

Table 4: 95% confidence interval results of the lower bound and the out-of-sample evaluation with 5000 disruption scenarios for 20 replication of policies obtained from Algorithm 1.

Table 4 shows that both lower bounds and out-of-sample evaluations are consistent, as the confidence interval radius among 20 replications is small. This provides a justification for the quality and precision of the obtained solution based on the selected cut generation rule from Section 4.1. However, the standard deviation within each replication of 5000 samples is large (in the magnitude of 1000), as different disruption times and magnitudes lead to significantly different sample path costs. In Algorithm 1 with $N' = 500$, the value of $\bar{z}$ varies significantly among iterations. In many

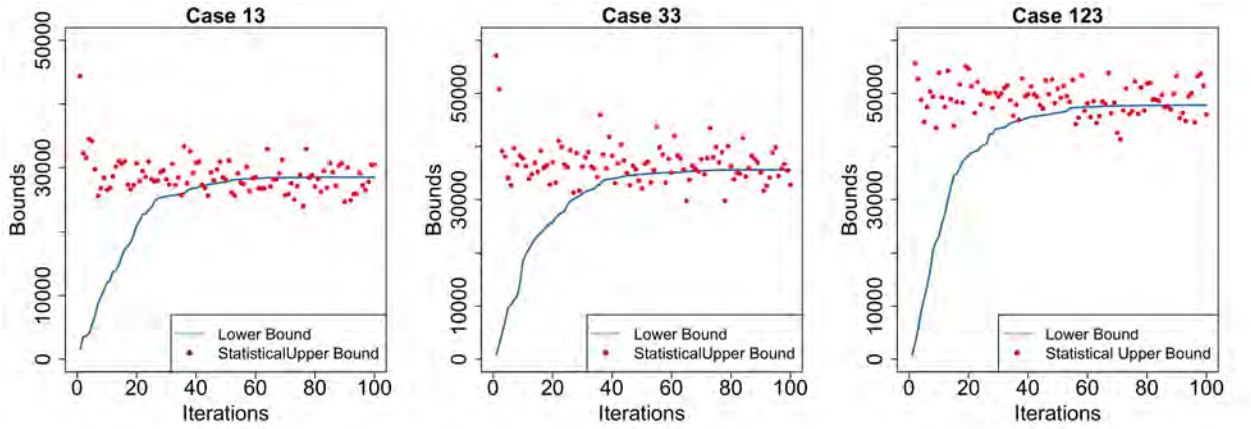

Figure 5: Lower bounds vs. statistical upper bounds of iterations for cut generation rules DOnly. In each iteration of Algorithm 1, the upper bound is obtained by evaluating the objective value with the current policy for 500 scenarios.

iterations we observe $\bar{z} < LB$ and a wide confidence interval $\mathcal{Z}$, due to the large variance. See Figure 5 for an illustration of how upper bounds and lower bounds progress. We omit $\mathcal{Z}$ in the figure as its lower ends are 0 and upper ends are approximately four times the statistical upper bound, which is too wide to provide useful information. Therefore, using termination criteria based on the statistical upper bound, either using the estimation $\bar{z}$ or its confidence interval $\mathcal{Z}$, can lead to premature termination of Algorithm 1.

4.3 Distribution Network Operational Insights

We examine under the stochastic disruption setting, how the objective value is affected by operational decisions such as installed battery capacity and battery utilization, pre-hardening a set of network components, and different lengths of disruption recovery times. Throughout this section we assume $T = 24$, $\tau = 4$, and $\lambda_D = \frac{1}{6}$ unless stated otherwise.

4.3.1 Battery Capacity and Utilization

We present in Table 5 the comparison of the installed battery capacity and the total amount of charging/discharging obtained by the stochastic policy and the deterministic alternative detailed in Section 4.2. We use 1000 sample paths to obtain the average total charge and discharge over the time horizon. In the deterministic policy, the installed battery capacity for a majority of locations is *zero*. The deterministic optimization model always chooses to directly satisfy demands using the conventional generators since it ignores the possibility of disruptions. The stochastic policy result shows that it is beneficial to install battery capacity and use batteries to prevent more expensive power mismatches in the network.

Similar to the result in Hari et al. (2018), the convex relaxation applied is tight with respect to

	Deterministic			Stochastic		
	Total Capacity (MW)	Avg. Total Charge (MWh)	Avg. Total Discharge (MWh)	Total Capacity (MW)	Avg. Total Charge (MWh)	Avg. Total Discharge (MWh)
Case 13	1.16	0.57	0.49	4.12	2.59	2.22
Case 33	0	0	0	0.70	0.81	0.71
Case 123	0	0.02	0	0.60	0.83	0.72

Table 5: Battery capacity and utilization comparison between the deterministic and stochastic policies for distribution network optimization with $N-1$ disruptions.

the efficiency curve. That is, the values of z^p and y either lie on or are very close to the efficiency curve in Figure 1. Suppose the efficiency curve has a function form $f^e(y)$. We define a tightness measure as $\Gamma = z^p/f^e(y)$ if $y \geq 0$ and $\Gamma = f^e(y)/z^p$ otherwise. The closer Γ is to 1, the closer the obtained z^p-y pair is to the efficiency curve. For each battery, we examine the average tightness measure over the time horizon, $\bar{\Gamma}_b$, $\forall b \in \mathcal{B}$. We observe a $\bar{\Gamma}_b > 0.95$ in more than 970 out of 1000 samples for all batteries except battery 6 and 7 in Case 13 and battery 1 in Case 123. For these exceptions, the lowest mean tightness measure across all samples is greater than 0.8. This observation corroborates that the convex relaxation is tight under most circumstances.

4.3.2 Hardening Network Components

Grid hardening can improve resiliency and prevent cascading failures (Nagarajan et al. 2016, Yamangil et al. 2015). In real-world applications, we can harden distribution lines and distributed generation by removing surrounding vegetation and constructing barriers. See Abel et al. (2004) for a detailed example. Here we perform a "what-if" analysis, testing the cost-effectiveness of protecting certain electrical components from the disruption. If a component is hardened, it is assumed that it will not fail when the disruption occurs at this component. We use the lower bound, LB, generated by Algorithm 1 as the costs. In Table 6, we present the percent of cost-saving of operating the hardened network versus operating the regular network without hardening, while both subject to stochastic $N-1$ disruptions.

Case 13			**Case 33**			**Case 123**		
Component	Cost ($)	% Cost saving	Component	Cost ($)	% Cost saving	Component	Cost ($)	% Cost saving
No hardening	5215.6	-	No hardening	10051.8	-	No hardening	13644.8	-
Line $(10, 13)$	3434.3	34.2	Line $(23, 24)$	3250.6	67.7	Line $(35, 40)$	7981.6	41.5
Line $(3, 4)$	4735.8	9.2	Generator 8	8830.9	12.1	Line $(13, 18)$	10893.2	20.2
Line $(8, 12)$	4747.3	9.0	Line $(20, 21)$	9292.0	7.6	Line $(7, 8)$	11474.9	15.9
Line $(1, 12)$	4846.5	7.1	Generator 1	9601.9	4.4	Line $(86, 87)$	12288.2	9.9
Line $(2, 7)$	5096.5	2.3	Line $(2, 3)$	9914.1	1.4	Line $(77, 78)$	12647.8	7.3

Table 6: Costs savings by hardening a component, compared to the no-hardening case. Five components with largest savings are selected.

For simplicity purposes, in each test case, we present only the five components with the largest saving in the optimal cost. The cost-saving can be considered as the price an operator is willing to pay for hardening. Table 6 suggests the importance of particular components such as lines and generators in sustaining resilience of the distribution network to $N-1$ disruptions. The benefit of hardening can be as large as 65% of the total cost but there is a major variance among all candidate components. In general, we observe that it can be beneficial to focus on the lines which lie directly between a generator and loads and lesser operating-cost generators with large capacities to maximize the benefit of hardening.

4.3.3 Effects of the Recovery Phase Duration

Understanding how the total cost changes as the recovery phase duration (τ) increases can be useful, particularly from the perspective of repair crew dispatch (Lei et al. 2019). In Table 7, for $\tau \in \{2, 4, 6, 8, 10\}$, we present the stochastic policy lower bound (LB) and an out-of-sample cost, $\bar{z}_{1000}$, obtained by evaluating the stochastic policy against 1000 sample paths with the corresponding recovery time. The result shows a longer recovery duration increases system costs. Table 7 indicates such an increasing trend of the total cost as τ increases for both LB and $\bar{z}_{1000}$. More than 10% of cost reduction can be achieved if the recovery time is reduced by 30 minutes, indicating the importance of a quick recovery. Note that the decreasing value of τ does not pose an exponential impact on Algorithm 1's run time, since both the recovery time and the frequency of disruptions (λ_D) govern the number of stages.

τ		2	4	6	8	10
Case 13	LB ($)	4120.7	5212.9	6383.4	7542.8	8586.1
	$\bar{z}_{1000}$ ($)	4225.4	5351.0	5858.0	7566.3	8804.2
	Time (sec.)	1285.6	896.4	600.3	487.8	391.7
Case 33	LB ($)	7606.4	10047.7	11830.4	13235.5	14303.1
	$\bar{z}_{1000}$ ($)	7237.2	9720.5	11694.4	12198.5	14182.6
	Time (sec.)	1700.0	1215.4	977.2	805.6	700.2
Case 123	LB ($)	10125.6	13643.0	16323.7	18560.5	20409.0
	$\bar{z}_{1000}$ ($)	10662.1	13066.6	15540.3	19831.2	19828.0
	Time (sec.)	2877.7	2343.6	1828.6	1586.4	1450.7

Table 7: Trend of the lower bound (LB) and simulated estimation costs ($\bar{z}_{1000}$) as the recovery duration, τ, increases.

We perform the following test with scenario-specific recovery times. For each test case, we select the five components from Table 6 to be subject to disruptions and there are three possible recovery time $\tau \in \{2, 4, 6\}$. For comparison, we obtain a policy assuming the recovery time is uniform at the mean value $\tau = 4$. We obtain the lower bound and the out-of-sample cost similar to Table 7, using the 1000 sample paths with scenario-specific recovery time. The results are shown in Table 8, with the lower bound and the out-of-sample test cost for the latter policy denoted as LB^U and $\bar{z}^U_{1000}$.

	LB (\$)	LB^U (\$)	$\bar{z}_{1000}$ (\$)	$\bar{z}^U_{1000}$ (\$)
Case 13	11916.2	11776.3	11678.7	11810.5
Case 33	32464.7	32697.8	32584.0	32734.0
Case 123	44891.6	43685.8	44905.0	43763.6

Table 8: Comparison of the lower bound and out-of-sample costs as for policies with and without consideration of various recovery times.

There are only five components subject to disruptions, so the probability of each component getting disrupted is larger compared to the original problem setting. The selected components are shown to have a significant economic impact in Table 6, which leads to the tripled lower bound. Policies' lower bounds vary case-by-case as the impact of recovery times may be different among test cases. However, the out-of-sample tests show that the policy assuming a uniform recovery time is less than 1% worse off than that assuming various recovery times, even better for Case 123. It shows that using the expected recovery time may be a good approximation when we have scenario-specific recovery time. It can reduce the size of Ω and enhance the computational performance since we only need to have one recovery time associated with each potentially disrupted component.

4.3.4 Multiple-component Stochastic Disruption Modeling

We now present additional tests to include scenarios in which multiple components can fail. In a large distribution network, it is likely to observe failures in multiple components during disruptions, such as natural disasters and extreme weather conditions (Byeon et al. 2020, Ma et al. 2019, Yan et al. 2019). We can extend our $N-1$ disruption setting to a more general one where there is a set of disrupted components for each scenario $\omega \in \Omega$. Here we compare three policies: (i) the deterministic policy assuming no disruption would occur, first described in Section 4.2 and denoted by "D"; (ii) the stochastic policy assuming $N-1$ disruptions denoted by "S"; and (iii) the stochastic policy assuming possible multiple-component disruptions denoted by "MS". We obtain their policy lower bounds and out-of-sample costs with 1000 scenarios of multiple-component disruptions. We show the test results for Case 123 in Table 9, with detailed scenario setup listed in Online Supplement A.

Case 123	D	S	MS
LB (\$)	470.3	13641.8	64724.8
$\bar{z}_{1000}$ (\$)	228578.2	70242.7	65295.6

Table 9: Cost of policies for disruptions with multiple failed components.

We observe from the lower bound results that the multiple-component disruptions lead to more severe economic losses compared to the single-component setting. The deterministic policy yields three times the cost compared to the stochastic policies, and the gap between the deterministic

policy and the stochastic ones is larger than that listed in Table 3. On the contrary, the out-of-sample tests show that the policy that protects against the $N-1$ disruptions is 7.0% more expensive compared to the optimal stochastic policy for the multi-component setting. The large number of multiple-component disruption scenarios, typically combinatorial in the network size, can render the problem computationally intractable. Since the number of $N-1$ disruption scenarios grows linearly in the number of components, the result in Table 9 shows that the policy for the $N-1$ disruption can still be a reasonable approximation for the multi-component setting with relatively moderate computational requirements.

5 Conclusions

We describe a multi-stage stochastic programming model that considers $N-1$ disruptions in a multi-period OPF problem for distribution networks. The model includes recovery time and other realistic physical features of distribution networks. An SDDP-based algorithm is developed to decompose the large-scale, recursive second-order cone formulation and the asymptotic convergence property is proved. The computational performance shows that our algorithm can obtain an optimal policy for large-scale test cases consistently within a reasonable time. The stochastic policy can be significantly cheaper than its deterministic counterpart. Analyses of battery capacities and their utilization, hardening critical network components and shortening the recovery duration provide the operational insights based on the stochastic-disruption-aware model in the real-world setting.

There remain many interesting future directions for this work. From the algorithmic perspective, it is important to determine the best cut generation rule used in Algorithm 1 in a theory-driven way. From the modeling perspective, in the first-stage problem, we can incorporate network and DER-placement design options via discrete decision variables, to which our SDDP-based algorithm still applies since convexity retains for all recourse problems. It is also useful but more challenging to incorporate repair crew dispatch decisions in the recourse problem. We need to introduce binary decision variables, which make all value functions for later stages noncontinuous and nonconvex. Finding a tight approximation to such recourse problems is crucial for future extensions.

When the rate of disruption occurring is small, which corresponds to a rare-event situation, the Monte Carlo simulation may not generate enough sample paths that represent a disruption. Importance sampling methods can be used to generate scenarios with disruptions in two-stage stochastic programming (Dantzig and Infanger 1993, Infanger 1992), but it requires more work on extending the limited literature on sequential decision problems (Dempster 2006) to our stochastic disruption setting.

It would be practical to extend our models to incorporate three-phase unbalanced distribution networks and adapt our algorithm to uncertainty at DER generations and loads, possibly incorporating distributionally robust optimization techniques. It will be important to scale the SDDP

algorithm to networks with thousands of buses and larger time horizons, potentially through adaptive sampling methods and linear approximation of second-order cone programs.

Acknowledgements

This work has been supported by Dan Ton's Advanced Grid Research Program, "Resilient Operation of Networked Microgrids" from the U.S. Department of Energy, Office of Electricity and the Center for Nonlinear Studies (CNLS) at Los Alamos National Laboratory. We thank the Center for Optimization and Statistical Learning at Northwestern University for the generous allotment of computing time on its clusters. The authors thank three anonymous referees and an associate editor, along with the area editor Dr. Pascal Van Hentenryck, for comments and suggestions that improved the paper.

References

A. Abel, P. W. Parfomak, and D. A. Shea. Electric utility infrastructure vulnerabilities: Transformers towers and terrorism. Technical Report R42795, Congressional Research Service, 2004.

A. Arab, A. Khodaei, S. K. Khator, K. Ding, V. A. Emesih, and Z. Han. Stochastic pre-hurricane restoration planning for electric power systems infrastructure. *IEEE Transactions on Smart Grid*, 6(2):1046–1054, 2015.

S. Babaei, R. Jiang, and C. Zhao. Distributionally robust distribution network configuration under random contingency. *arXiv preprint:1808.09038*, 2018. URL `https://arxiv.org/abs/1808.09038`.

C. Bandi, D. Krishnamurthy, D. P. Morton, and H. Yang. Robust optimization for electricity generation. *arXiv preprint:1803.06984*, 2019. URL `https://arxiv.org/abs/1803.06984`.

M. Baran and F. F. Wu. Optimal sizing of capacitors placed on a radial distribution system. *IEEE Transactions on Power Delivery*, 4(1):735–743, 1989.

M. E. Baran and F. F. Wu. Network reconfiguration in distribution systems for loss reduction and load balancing. *IEEE Transactions on Power Delivery*, 4(2):1401–1407, 1989.

A. Barnes, H. Nagarajan, E. Yamangil, R. Bent, and S. Backhaus. Resilient design of large-scale distribution feeders with networked microgrids. *Electric Power Systems Research*, 171:150–157, 2019.

D. Bienstock. *Electrical Transmission System Cascades and Vulnerability: An Operations Research Viewpoint*. SIAM, 2015.

D. Bienstock, C. Matke, G. Muñoz, and S. Yang. Robust linear control of nonconvex battery operation in transmission systems. *arXiv preprint:1610.09432*, 2016. URL `https://arxiv.org/abs/1610.09432`.

J. R. Birge and F. V. Louveaux. A multicut algorithm for two-stage stochastic linear programs. *European Journal of Operational Research*, 34:384–392, 1988.

G. G. Brown, W. M. Carlyle, J. Salmerón, and K. Wood. Analyzing the vulnerability of critical infrastructure to attack and planning defenses. In *Emerging Theory, Methods, and Applications*, pages 102–123. INFORMS, 2005.

Geunyeong Byeon, Pascal Van Hentenryck, Russell Bent, and Harsha Nagarajan. Communication-constrained expansion planning for resilient distribution systems. *INFORMS Journal on Computing*, 2020. URL `https://doi.org/10.1287/ijoc.2019.0899`.

M. B. Cain, R. P. O'Neill, and A. Castillo. History of optimal power flow and formulations. Technical report, Federal Energy Regulatory Commission, 2012.

G. Cardoso, M. Heleno, and N. DeForest. Remote off-grid microgrid design support tool (ROMDST) - an optimal design support tool for remote, resilient, and reliable microgrids (Phase II, Final Report). Technical report, Lawrence Berkeley National Laboratory, 2019.

S. Chalil Madathil, E. Yamangil, H. Nagarajan, A. Barnes, R. Bent, S. Backhaus, S. J. Mason, S. Mashayekh, and M. Stadler. Resilient off-grid microgrids: Capacity planning and N-1 security. *IEEE Transactions on Smart Grid*, 9(6):6511–6521, 2018.

Q. Chen. *The probability, identification, and prevention of rare events in power systems.* PhD thesis, Iowa State University, 2004.

Z. Chen and W. B. Powell. Convergent cutting-plane and partial-sampling algorithm for multistage stochastic linear programs with recourse. *Journal of Optimization Theory and Applications*, 102:497–524, 1999.

J. Choi, T. D. Mount, and R. J. Thomas. Transmission expansion planning using contingency criteria. *IEEE Transactions on Power Systems*, 22(4):2249–2261, 2007.

G. B. Dantzig and G. Infanger. Approaches to stochastic programming with application to electric power systems. In *Optimization in Planning and Operation of Electric Power Systems*, pages 125–138. Springer, 1993.

M. A. H. Dempster. Sequential importance sampling algorithms for dynamic stochastic programming. *Journal of Mathematical Sciences*, 133(4):1422–1444, 2006.

L. Ding, S. Ahmed, and A. Shapiro. A python package for multi-stage stochastic programming. *Optimization Online*, 2019. URL `http://www.optimization-online.org/DB_FILE/2019/05/7199.pdf`.

O. Dowson. The policy graph decomposition of multistage stochastic optimization problems. *Optimization Online*, 2018. URL `http://www.optimization-online.org/DB_HTML/2018/11/6914.html`.

O. Dowson and L. Kapelevich. SDDP.jl: a Julia package for stochastic dual dynamic programming. *Optimization Online*, 2017. URL `http://www.optimization-online.org/DB_HTML/2017/12/6388.html`.

I. Dunning, J. Huchette, and M. Lubin. JuMP: A modeling language for mathematical optimization. *SIAM Review*, 59:295–320, 2017.

Executive Office of the President. Economic benefits of increasing electric grid resilience to weather outages. Technical report, Executive Office of the President, 2013.

A. Frangioni and C Gentile. Solving nonlinear single-unit commitment problems with ramping constraints. *Operations Research*, 54(4):767–775, 2006.

L. Gan, N. Li, U. Topcu, and S. H. Low. Exact convex relaxation of optimal power flow in radial networks. *IEEE Transactions on Automatic Control*, 60(1):72–87, 2014.

P. Girardeau, V. Leclère, and A. B. Philpott. On the convergence of decomposition methods for multistage stochastic convex programs. *Mathematics of Operations Research*, 40(1):130–145, 2014.

Lawrence Berkeley National Laboratory Grid Integration Group. The distributed energy resources customer adoption model (der-cam), 2020. URL `https://gridintegration.lbl.gov/der-cam`.

Gurobi Optimization, Inc. *Gurobi Reference Manual*, 2016. URL `http://www.gurobi.com`.

S. K. K. Hari, K. Sundar, H. Nagarajan, R. Bent, and S. Backhaus. Hierarchical predictive control algorithms for optimal design and operation of microgrids. In *Power Systems Computation Conference (PSCC)*, pages 1–7. IEEE, 2018.

K. W. Hedman, R. P. O'Neill, E. B. Fisher, and S. S. Oren. Optimal transmission switching with contingency analysis. *IEEE Transactions on Power Systems*, 24(3):1577–1586, 2009.

G. Infanger. Monte carlo (importance) sampling within a benders decomposition algorithm for stochastic linear programs. *Annals of Operations Research*, 39(1):69–95, 1992.

S. Lei, C. Chen, Y. Li, and Y. Hou. Resilient disaster recovery logistics of distribution systems: Co-optimize service restoration with repair crew and mobile power source dispatch. *IEEE Transactions on Smart Grid*, 10(6):6187–6202, Nov 2019.

Z. Lin, Z. Hu, and Y. Song. Distribution network expansion planning considering N-1 criterion. *IEEE Transactions on Power Systems*, 34(3):2476–2478, 2019.

K. Linowsky and A. B. Philpott. On the convergence of sampling-based decomposition algorithms for multistage stochastic programs. *Journal of Optimization Theory and Applications*, 125(2): 349–366, 2005.

S. Ma, S. Li, Z. Wang, and F. Qiu. Resilience-oriented design of distribution systems. *IEEE Transactions on Power Systems*, 34(4):2880–2891, 2019.

S. Mashayekh, M. Stadler, G. Cardoso, M. Heleno, S. C. Madathil, H. Nagarajan, R. Bent, M. Mueller-Stoffels, X. Lu, and J. Wang. Security-constrained design of isolated multi-energy microgrids. *IEEE Transactions on Power Systems*, 33(3):2452–2462, 2017.

H. Nagarajan, E. Yamangil, R. Bent, P. Van Hentenryck, and S. Backhaus. Optimal resilient transmission grid design. In *Power Systems Computation Conference (PSCC)*, pages 1–7. IEEE, 2016.

M. V. F. Pereira and L. M. V. G. Pinto. Multi-stage stochastic optimization applied to energy planning. *Mathematical programming*, 52(1-3):359–375, 1991.

A. B. Philpott and Z. Guan. On the convergence of stochastic dual dynamic programming and related methods. *Operations Research Letters*, 36(4):450–455, 2008.

S. Rebennack. Combining sampling-based and scenario-based nested Benders decomposition methods: application to stochastic dual dynamic programming. *Mathematical Programming*, 156 (1):343–389, 2016.

R. T. Rockafellar and R. J-B. Wets. Stochastic convex programming: Relatively complete recourse and induced feasibility. *SIAM Journal on Control and Optimization*, 14(3):574–589, 1976.

J. Salmerón, R. K. Wood, and D. P. Morton. A stochastic program for optimizing military sealift subject to attack. *Military Operations Research*, 14(2):19–39, 2009.

K. P. Schneider, B. A. Mather, B. C. Pal, C. . Ten, G. J. Shirek, H. Zhu, J. C. Fuller, J. L. R. Pereira, L. F. Ochoa, L. R. de Araujo, R. C. Dugan, S. Matthias, S. Paudyal, T. E. McDermott, and W. Kersting. Analytic considerations and design basis for the ieee distribution test feeders. *IEEE Transactions on Power Systems*, 33(3):3181–3188, 2018.

A. Shapiro. Analysis of stochastic dual dynamic programming method. *European Journal of Operational Research*, 209(1):63–72, 2011.

A. Shapiro, D. Dentcheva, and A. Ruszczyński. *Lectures on stochastic programming: modeling and theory*. SIAM, 2009.

D. T. Ton and W. T. P. Wang. A more resilient grid: The US department of energy joins with stakeholders in an R&D plan. *IEEE Power and Energy Magazine*, 13(3):26–34, 2015.

M. Vanin, H. Ergun, R. Dhulst, and D. Van Hertem. Comparison of linear and conic power flow formulations for unbalanced low voltage network optimization. *Electric Power Systems Research*, 189:106699, 2020.

Emre Yamangil, Russell Bent, and Scott Backhaus. Resilient upgrade of electrical distribution grids. In *Twenty-Ninth AAAI Conference on Artificial Intelligence*, 2015.

J. Yan, B. Hu, K. Xie, J. Tang, and H. Tai. Data-driven transmission defense planning against extreme weather events. *IEEE Transactions on Smart Grid*, 11(3):2257–2270, 2019.

H. Yang and D. P. Morton. Optimal crashing of an activity network with disruptions. *Optimization Online*, 2019. URL `http://www.optimization-online.org/DB_HTML/2019/10/7403.html`.

Haoxiang Yang and Harsha Nagarajan. Optimal power flow in distribution networks under stochastic N-1 disruptions. *Electric Power Systems Research*, 189:106689, 2020.

W. Yuan, J. Wang, F. Qiu, C. Chen, C. Kang, and B. Zeng. Robust optimization-based resilient distribution network planning against natural disasters. *IEEE Transactions on Smart Grid*, 7(6):2817–2826, 2016.

H. Zhou, J. H. Zheng, Z. Li, Q. H. Wu, and X. X. Zhou. Multi-stage contingency-constrained co-planning for electricity-gas systems interconnected with gas-fired units and power-to-gas plants using iterative benders decomposition. *Energy*, 180:689–701, 2019.

Online Supplement

Online Supplement A Test Case Construction and Parameter Selection

Due to the limited space of this paper, we present all data of Case 13 and the component subject to disruptions in Case 123. Case 33 and Case 123 have the same data structure and all detailed data files can be found in the GitHub repository (`https://github.com/haoxiangyang89/Distribution_Disruption_Supplement`). We include network topology, generator locations and costs, battery locations and their features, distribution line specifications, components subject to disruptions, and a load profile. Each case has one generator with large capacity and small costs, which serves as the approximation of the feeder between the transmission network and the distribution network.

Case 13:

- Network topology:

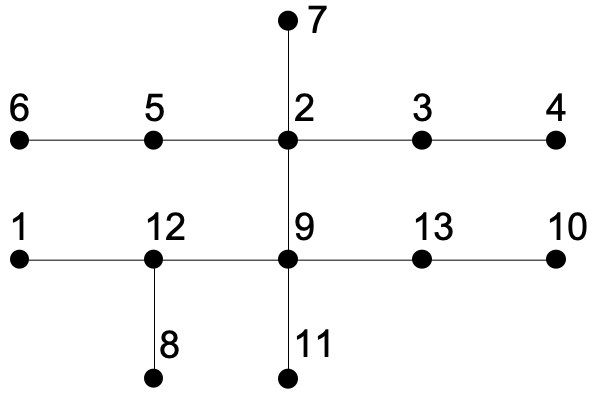

Figure 6: Distribution network of Case 13.

- The base voltage for all buses is 4.16KV. The squared voltage bounds are $\bar{V}_i = 1.05^2, \underline{V}_i = 0.95^2,\ \forall i \in \mathcal{N}$, in per unit (p.u.).
- Generator data: $c^l = 10000$

Location	$\bar{s}_g^p$	$\bar{s}_g^q$	$\underline{s}_g^p$	$\underline{s}_g^p$	$c_{g,1}$	$c_{g,2}$	R_g^U	R_g^D
3	2.5	2.5	0	-2.5	5	10	6	-6
5	2.75	2.5	0	-2.5	10	20	6	-6
7	10	8	0	-8	2	1	20	-20
12	2.25	2.5	0	-2.5	20	40	6	-6
13	2.25	2.5	0	-2.5	20	40	6	-6

- Battery data: for all batteries $b \in \mathcal{B}$,

- $|\mathcal{L}_b| = 4$;
- $\alpha_b^1 = 2,\ \alpha_b^2 = 1.067,\ \alpha_b^3 = 0.938,\ \alpha_b^4 = 0.5$;
- $\beta_b^1 = 0.7467,\ \beta_b^2 = 0,\ \beta_b^3 = 0,\ \beta_b^4 = 0.35$;
- $\bar{I}_b = 1$;
- $\bar{u}_b = 1$;
- $c_b^B = 130$;

- Line specifications:

Line (i,j)	W_{ij} (MVA)	R_{ij} (p.u.)	X_{ij} (p.u.)
(1,12)	0.9568	0.00653	0.00662
(2,3)	4.2432	0.01226	0.01962
(2,5)	1.9136	0.02174	0.02216
(2,7)	9.1104	0.02241	0.06775
(2,9)	9.1104	0.02241	0.06775
(3,4)	9.1104	0.00011	0.00034
(5,6)	1.9136	0.01304	0.01329
(8,12)	1.2896	0.03520	0.01344
(9,11)	9.1104	0.01120	0.03387
(9,12)	1.9136	0.01304	0.01329
(9,13)	9.1104	0.00011	0.00034
(10,13)	4.1059	0.01303	0.00708

- Components subject to disruptions: all generators and lines

- Demand profile: the demand profiles for active and reactive power are generated from a normal distribution where the mean equals to the following base demand, $d_i^{p,0}$ and $d_i^{q,0}$, and the standard deviation is half of the base demand. If the randomly generated active demand is smaller than 0, we force it to take value 0. The unit is MW for the active demand and MVAr for the reactive demand.
  - $d_1^{p,0} = 0.021,\ d_2^{p,0} = 0.12,\ d_4^{p,0} = 0.438,\ d_5^{p,0} = 0.631,\ d_6^{p,0} = 0.039,\ d_8^{p,0} = 0.12,$ $d_9^{p,0} = 3.002,\ d_{10}^{p,0} = 0.586,\ d_3^{p,0} = d_7^{p,0} = d_{11}^{p,0} = d_{12}^{p,0} = d_{13}^{p,0} = 0$
  - $d_1^{q,0} = 0.013,\ d_2^{q,0} = 0.0744,\ d_4^{q,0} = 0.271,\ d_5^{q,0} = 0.391,\ d_6^{q,0} = 0.0242,\ d_8^{q,0} = 0.0892,$ $d_9^{q,0} = 1.861,\ d_{10}^{q,0} = 0.363,\ d_3^{q,0} = d_7^{q,0} = d_{11}^{q,0} = d_{12}^{q,0} = d_{13}^{q,0} = 0$

Case 123: Disruption scenarios

- $N-1$ setting:

– Generators at bus: 1, 25, 35, 60, 76, 97, 108, 116

– Lines: (7,8), (13,18), (25,26), (35,40), (67,97), (57,60), (86,87), (77,78), (105,108)

- Multiple component setting scenarios:

1. Line (7,8), (13,18), Generator at bus 1
2. Line (35,40), Generator at bus 35
3. Line (57,60), Generator at bus 60
4. Line (25,26), Generator at bus 25
5. Line (77,78), Generator at bus 76
6. Line (105,108), Generators at bus 97 and 108
7. Line (67,97), Generators at bus 1 and 116

Online Supplement B Dual Formulation of Model (2)

In this section we present the formulation of the dual problem of model (2), and then we explain the corresponding relationship between the dual variables and the primal constraints in model (2).

$$
\begin{aligned}
\max \quad & \sum_{t=t_D}^{T} \Bigg[- \sum_{g \in \mathcal{G}} \Big(\bar{s}_g^p B_{gt}^{\omega} \lambda_{gt}^{spu} + \underline{s}_g^p B_{gt}^{\omega} \lambda_{gt}^{spl} + \bar{s}_g^q B_{gt}^{\omega} \lambda_{gt}^{squ} + \underline{s}_g^q B_{gt}^{\omega} \lambda_{gt}^{sql} + R_g^U B_{gt}^{\omega} \lambda_{gt}^{RU} + R_g^D B_{gt}^{\omega} \lambda_{gt}^{RD} \Big) - \\
& \sum_{i \in \mathcal{N}} \Big(\bar{V}_i \lambda_{it}^{vu} + \underline{V}_i \lambda_{it}^{vl} + d_{it}^p \lambda_{it}^{pd} + d_{it}^q \lambda_{it}^{qd} \Big) - \sum_{k \in \mathcal{E}} W_k B_{kt}^{\omega} \nu_{1,kt} - \sum_{b \in \mathcal{B}} \left(\bar{I}_b \lambda_b^{wu} + \sum_{\ell \in \mathcal{L}_b} \beta_b^{\ell} \lambda_{blt}^{\alpha\beta} \right) \Bigg] - \\
& \sum_{g \in \mathcal{G}} \hat{s}_{gt_D-1}^p \gamma_g - \sum_{b \in \mathcal{B}} (\bar{u}_b \lambda_b^{uu} + \hat{u} \zeta_b + \hat{w}_{bt_D-1} \eta_b) - \sum_{\omega \in \Omega} \sum_{t=t_D+\tau^{\omega}+1}^{T} \sum_{l \in \mathcal{C}_t^{\omega}} \lambda_{t\omega l}^c \Big(\hat{v}^{t\omega l} - {\gamma^{t\omega l}}^{\top} \hat{s}_{\cdot t-1}^{p,t\omega l} - \\
& {\eta^{t\omega l}}^{\top} \hat{w}_{\cdot t-1}^{t\omega l} - {\zeta^{t\omega l}}^{\top} \hat{u}^{t\omega l} \Big) - \sum_{t=t_D}^{T} \left[\sum_{g \in \mathcal{G}} \left(\frac{c_{g1}^2 - c_{g2}}{4c_{g2}} \mu_{31,gt} + \frac{c_{g1}}{2\sqrt{c_{g2}}} \mu_{32,gt} + \frac{c_{g1}^2 + c_{g2}}{4c_{g2}} \nu_{3,gt} \right) \right] \qquad (15a)
\end{aligned}
$$

$$
\begin{aligned}
\text{s.t.} \quad & \lambda_{gt}^{spu} + \lambda_{gt}^{spl} + \lambda_{i_g t}^{pd} + B_{gt}^{\omega} \lambda_{gt}^{RU} - B_{gt+1}^{\omega} \lambda_{gt+1}^{RU} + B_{gt}^{\omega} \lambda_{gt}^{RD} - B_{gt+1}^{\omega} \lambda_{gt+1}^{RD} - \sqrt{c_{g2}} \mu_{32,gt} - \\
& \sum_{\omega \in \Omega} \sum_{\substack{l \in \mathcal{C}_{t+1}^{\omega}: \\ t \geq t_D + \tau^{\omega}}} \lambda_{t+1\omega l}^c \gamma_g^{t+1\omega l} = 0 \qquad \forall g \in \mathcal{G}, t = t_D, \ldots, T-1 \quad (15b) \\
& \lambda_{gT}^{spu} + \lambda_{gT}^{spl} + \lambda_{i_g T}^{pd} + B_{gT}^{\omega} \lambda_{gT}^{RU} + B_{gT}^{\omega} \lambda_{gT}^{RD} - \sqrt{c_{g2}} \mu_{32,gT} = 0 \qquad \forall g \in \mathcal{G} \quad (15c) \\
& B_{gt_D}^{\omega} \lambda_{gt_D}^{RU} + B_{gt_D}^{\omega} \lambda_{gt_D}^{RD} + \gamma_g = 0 \qquad \forall g \in \mathcal{G} \quad (15d) \\
& \lambda_{gt}^{squ} + \lambda_{gt}^{sql} + \lambda_{i_g t}^{qd} = 0 \qquad \forall g \in \mathcal{G}, t = t_D, \ldots, T \quad (15e) \\
& -\lambda_{it}^{pd} + R_k B_{kt}^{\omega} \lambda_{kt}^{pf} - B_{kt}^{\omega} \mu_{11,kt} = 0 \qquad \forall k = ij \in \mathcal{E}, t = t_D, \ldots, T \quad (15f) \\
& -\lambda_{it}^{qd} + X_k B_{kt}^{\omega} \lambda_{kt}^{pf} - B_{kt}^{\omega} \mu_{12,kt} = 0 \qquad \forall k = ij \in \mathcal{E}, t = t_D, \ldots, T \quad (15g) \\
& \lambda_{it}^{vu} + \lambda_{it}^{vl} + \sum_{k=ji \in \mathcal{E}} B_{kt}^{\omega} \lambda_{kt}^{pf} - \sum_{k=ij \in \mathcal{E}} B_{kt}^{\omega} \lambda_{kt}^{pf} = 0 \qquad \forall i \in \mathcal{N}, t = t_D, \ldots, T \quad (15h) \\
& -c_{it}^L \leq \lambda_{it}^{pd} \leq c_{it}^L \qquad \forall i \in \mathcal{N}, t = t_D, \ldots, T \quad (15i)
\end{aligned}
$$

$$-c^L_{it} \le \lambda^{qd}_{it} \le c^L_{it} \qquad \forall i \in \mathcal{N}, t = t_D, \dots, T \qquad (15j)$$

$$\lambda^{wu}_{bt} + \lambda^I_{bt} - \lambda^I_{bt+1} - \sum_{\omega \in \Omega} \sum_{\substack{l \in \mathcal{C}^\omega_{t+1}: \\ t \ge t_D + \tau^\omega}} \lambda^c_{t+1\omega l} \eta^{t+1\omega l}_b = 0 \qquad \forall b \in \mathcal{B}, t = t_D, \dots, T-1 \qquad (15k)$$

$$\lambda^{wu}_{bT} + \lambda^I_{bT} \ge 0 \qquad \forall b \in \mathcal{B} \qquad (15l)$$

$$\eta_b - \lambda^I_{bt_D} \ge 0 \qquad \forall b \in \mathcal{B} \qquad (15m)$$

$$\lambda^{uu}_b + \zeta_b - \sum_{t=t_D}^{T} \nu_{2,bt} - \sum_{\omega \in \Omega} \sum_{\substack{l \in \mathcal{C}^\omega_{t+1}: \\ t \ge t_D + \tau^\omega}} \lambda^c_{t+1\omega l} \zeta^{t+1\omega l}_b \ge 0 \qquad \forall b \in \mathcal{B} \qquad (15n)$$

$$\lambda^{pd}_{i_b t} + \sum_{\ell \in \mathcal{L}_b} \lambda^{\alpha\beta}_{blt} - \mu_{21,bt} = 0 \qquad \forall b \in \mathcal{B}, t = t_D, \dots, T \qquad (15o)$$

$$\lambda^{qd}_{i_b t} - \mu_{22,bt} = 0 \qquad \forall b \in \mathcal{B}, t = t_D, \dots, T \qquad (15p)$$

$$\Delta t \lambda^I_{bt} - \sum_{\ell \in \mathcal{L}_b} \alpha^\ell_b \lambda^{\alpha\beta}_{blt} = 0 \qquad \forall b \in \mathcal{B}, t = t_D, \dots, T \qquad (15q)$$

$$\sum_{l \in \mathcal{C}^\omega_t} \lambda^c_{t\omega l} \ge -c^\theta_{t\omega} \qquad \forall \omega \in \Omega, t = t_D + \tau^\omega + 1, \dots, T \qquad (15r)$$

$$\mu_{31,gt} + \nu_{3,gt} \le c^h_{gt} \qquad \forall g \in \mathcal{G}, t = t_D, \dots, T \qquad (15s)$$

$$\|(\mu_{11,kt}, \mu_{12,kt})\| \le \nu_{1,kt} \qquad \forall k \in \mathcal{E}, t = t_D, \dots, T \qquad (15t)$$

$$\|(\mu_{21,kt}, \mu_{22,kt})\| \le \nu_{2,kt} \qquad \forall k \in \mathcal{E}, t = t_D, \dots, T \qquad (15u)$$

$$\|(\mu_{31,kt}, \mu_{32,kt})\| \le \nu_{3,kt} \qquad \forall k \in \mathcal{E}, t = t_D, \dots, T \qquad (15v)$$

$$\lambda^{spu}, \lambda^{squ}, \lambda^{vu}, \lambda^{wu}, \lambda^{uu}, \lambda^{RU}, \lambda^{\alpha\beta}, \nu_1, \nu_2, \nu_3 \ge 0 \qquad (15w)$$

$$\lambda^{spl}, \lambda^{sql}, \lambda^{vl}, \lambda^{RD} \le 0. \qquad (15x)$$

As stated in Section 3, we denote the index set of cuts generated for a specific (t, ω) pair as $\mathcal{C}^\omega_t$. In this formulation, λ^{pd} and λ^{qd} are the dual variables of flow balance constraints (2b) and (2c). Power flow equations (2e) and (2f) can be reformulated as an equality just for the functional lines, with the corresponding dual variable λ^{pf}. We use λ^{RU} and λ^{RD} to represent the dual variables of the ramping constraints (2g) and (2h), $\lambda^{spu}, \lambda^{spl}, \lambda^{squ}$ and λ^{sql} to represent the dual variables corresponding to the upper and lower bounds for power generation (2i)-(2j), and λ^{vu} and λ^{vl} to represent the dual variables corresponding to the upper and lower bounds for squared voltage (2k). For constraints on batteries, we denote the dual variables for constraints (2l), (2n)-(2p) as $\lambda^I, \lambda^{\alpha\beta}, \lambda^{wu}$ and λ^{uu}, respectively. Dual variables γ, η and ζ correspond to the non-anticipativity constraints (2r)-(2t). As we generate cuts to approximate the value function f from below, the dual variables for those cuts are denoted as λ^c.

Finally, suppose we create an auxiliary variable h_{gt} to represent the generation cost at generator $g \in \mathcal{G}$ for time $t = t_D, \dots, T$. We can then introduce a set of second-order cone constraints as follows to characterize this quadratic cost function:

$$c_{g2} {s^p_{gt}}^2 + c_{g1} s^p_{gt} \le h_{gt} \quad \iff \quad \|(h_{gt} + \frac{c^2_{g1} - c_{g2}}{4c_{g2}}, \sqrt{c_{g2}} s^p_{gt} + \frac{c_{g1}}{2\sqrt{c_{g2}}})\| \le h_{gt} + \frac{c^2_{g1} + c_{g2}}{4c_{g2}}. \qquad (16)$$

For the second-order cone constraints (2d), (2m) and (16), we employ three sets of dual variables as (μ_1, ν_1), (μ_2, ν_2) and (μ_3, ν_3). The dual SOCP constraints are formed as (15t)-(15v).

With the dual variables established, we build constraint (15b)-(15d) for the primal variable s^p (for time $t_D, \ldots, T, T$ and $t_D - 1$), (15e) for s^q, (15h) for V, (15i) and (15j) for L^{p+}, L^{p-}, L^{q+} and L^{q-}, (15k)-(15m) for w (for time $t_D, \ldots, T, T$ and $t_D - 1$), (15n) for u, (15o) and (15p) for z^p and z^q, (15q) for y, (15r) for the approximated value function term θ, and (15s) for the auxiliary variables h. Here for simplicity of representation, we define the coefficients in the primal objective function for L, θ and h terms as c^L, c^θ and c^h, which can be calculated from the probability parameters p_t^ω and the penalty coefficient c^l.

Online Supplement C Cut Pre-generation

In the first few iterations of an SDDP-type algorithm, cuts (7) may be loose for earlier stages as they have coarse approximation of later-stage value functions in their objective functions. However, these cuts are tight approximations for any terminal stage value function from the beginning of the algorithm. The terminal stage value functions in our problem are $f_t^\omega, \forall t \geq T - \tau + 1, \omega \in \Omega$. We can use this property to pre-generate cuts for terminal stage value functions so that the cuts for earlier stages are better from the beginning of the algorithm. We compare the run-time with and without the pre-generated cuts, as shown in Figure 7. For this test, we pre-generate 5 cuts in each iteration for 20 iterations before Algorithm 1. Although the pre-generation incurs an overhead and iterations with longer run-time towards the end, it helps achieve a better lower bound result if only a small sample budget is given.

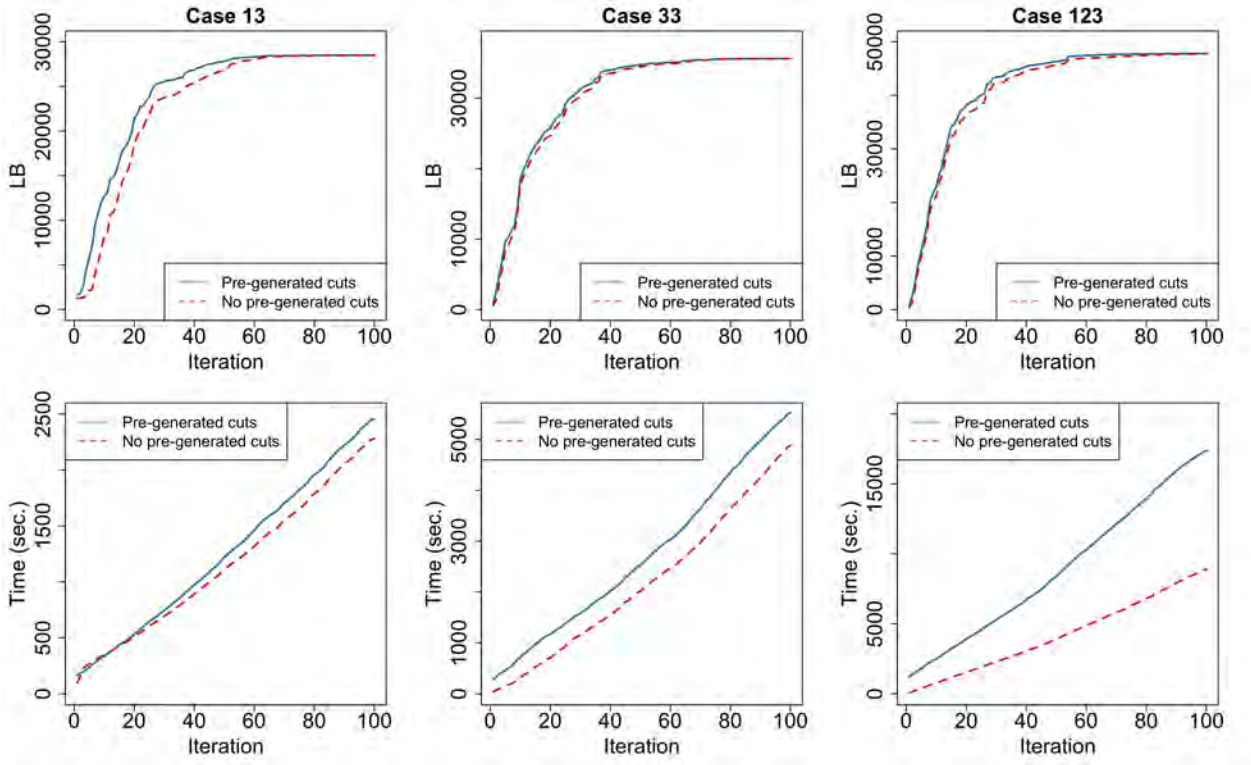

Figure 7: Lower bounds and run-times vs. the number of iterations with and without the terminal stage cut pre-generation. Five cuts are pre-generated in each iteration for 20 iterations.

.